A Discontinuous ALE formulation (DiscALE) for the modeling of polygonal mesh (r,h)-adaptation in finite volume context

Philippe Hoch

A Discontinuous ALE formulation (DiscALE) for the modeling of polygonal mesh (r,h)-adaptation in finite volume context

P. Hoch*

September 16, 2014

Abstract

We introduce a finite volume *Discontinuous Arbitrary Lagrangian-Eulerian* (*DiscALE*) alternative to the computation of compressible fluid dynamics. This new proposed framework take naturally into account dynamical refinement/coarsening/reconnection on a direct discretization of a new **non-smooth kinematic** mesh contribution. Two practical interesting properties of the method are -1- to deal with arbitrary polygonal mesh (initial or at each time step) and -2- to recover exactly Lagrangian, Eulerian or classical continuous ALE mode by omitting this non-smooth velocity. Moreover, it also appears that many meshing tools techniques can be seen as a direct discretization of this new discontinuous kinematic equation on a generic edge based patch. In this context, polygonal ALE-AMR (conformal or not) as well as edge swapping on simplices are special cases. Moreover, all underlying local mesh modification must verify a natural locality hypothesis (CFL constraint) and all associated Discrete Geometric Conservation Laws (DGCL) are exactly solved without computing any polygons/polygons intersections. The classical remapping fluxing scheme (swept or self intersection) has been extended to take into account the topological transformation of the boundary between two adjacent cells that generalize simplicial swapping to polygons.

keywords:
Discontinuous kinematic of mesh, ALE-AMR, arbitrary mesh reconnection, (r,h)-adaptation, refinement/coarsening, boundary transformation between two adjacent cells as generalized swapping, mesh sliding, DGCL.

1 Introduction

The aim of the paper is mainly to introduce an extension of Arbitrary-Lagrangian-Eulerian (ALE) standard continuous speed frame on unstructured polygonal

*CEA-DAM, DIF, F 91297, Arpajon, France (philippe.hoch@cea.fr)

cells in a finite volume context. This techniques offer many advantages with respect to purely Lagrangian or Eulerian computations by trying to get using benefits of local smoothing or concentrate nodes on regions of interest (using "error estimates"). Nevertheless, it may sometimes happen that some cells need to be removed or added, for meshing community, this is often called h-adaptation (see [23]). Classical hypothesis on ALE -continuous velocity- only permits to deal with r-adaptation (Cauchy-Lipschitz theorem) not with h-adaptation: refinement/coarsening and swapping are not allowed theoretically.
We are naturally led to consider *discontinuous* mesh motion, and then introducing Discontinuous-Arbitrary-Lagrangian-Eulerian framework (DiscALE). In this context the mesh connectivity evolution may also be itself arbitrary. The weaker hypothesis on spatial regularity of the mesh velocity enable topological changes, hence previous works on ALE-AMR [4, 34] are embedded in this discontinuous concept. Moreover, this new kinematic is coupled with exact local Discrete Geometrical Conservation Laws (DGCL) schemes. It turns out that the system of equations can be discretized on arbitrary unstructured polygonal and semi conformal cells. Semi-conformal polygons appear naturally as a representation of this refinement/coarsening phase, in each case, this gives raise to a different number of cells. This kind of adaptation may not be sufficient in some cases because of high mesh distortion as noticed in [30][16]. To circumvent this situation for general polygons, we have introduced a new concept of two adjacent cell border transformation that generalizes diagonal swapping for simplicial meshes [10, 7, 1, 16] moreover it appears that our reconnection approach is more local than ReALE (ALE with reconnection) [30] where Voronoy mesh is employed at each time step. We emphasize that a standard ALE scheme can be recovered (specially Eulerian mode can be exactly recovered).
The paper is organized as follows, in the first chapter we introduce the formal Discontinuous Arbitrary-Lagrangian-Eulerian framework, the prototype of interest systems are compressible Gaz Dynamics Euler equations. In the second step, we define some notations and introduce the central object that permits to deal with local mesh h-adaptation. We show that this framework include the ALE-AMR, refinement/coarsening, and may contain metric based approach. In a third step, we propose a new natural extension of swapping techniques to polygonal and/or semi conformal cells by a discretization of a local continuous optimization problem involving two adjacent cells. Mesh sliding is also recovered as a direct consequence. Besides this mesh modifications, two extensions of local remapper devoted to DGCL are proposed. Finally, in a fourth chapter, we show some numerical results.

2 Equations with Discontinuous Grid Velocity

In this section, we present the ALE framework based on the two dimensional Euler equations of gaz dynamics approximated on a domain moving at an arbitrary velocity, allowing continuous and discontinuous regularity for grid velocity. We briefly recall the basis fundamentals of ALE (smooth) framework, for a general

introduction, we refer also to [19] [31], we mainly follow the approach of [18].

2.1 Continuous view point

Two classical description of non relativistic continuum mechanics are (see Figures 1 and 2):

- material configuration Ω_X describing physical material particles. The Lagrangian approach consists in following a material particle in his motion, especially a mesh node can always identify to the same material point. By construction such an approach is not robust enough when dealing with large shear and vortexes.
- spatial configuration Ω_x describing spatial points. The Eulerian approach consists in decoupling mesh nodes (fixed) from material particles adding convective terms to pde description. Difficulties may appear in following interfaces and free boundaries problems.

The Arbitrary Lagrangian-Eulerian view point is a generalization that encompasses both configurations. It plays the role of a reference configuration Ω_ξ describing a new computational referential (which described mesh nodes after discretization), the bibliography on such method applied to compressible fluids flows is huge (see [19][24][14][17][32][18]).

We denote by $\mathbf{\Phi}$ the diffeomorphic map (bijective and bi-continuous) between initial and fixed Eulerian coordinates:

$$\begin{aligned} &\mathbf{\Phi} : \Omega_{s,\mathbf{X}} \to \Omega_{\mathbf{x}}, \\ &\quad (s, \mathbf{X}) \to (t, \mathbf{x}) = \mathbf{\Phi}(s, \mathbf{X}). \end{aligned} \tag{1}$$

The law of motion linking both material $\mathbf{X}$ and spatial $\mathbf{x}$ particles in time :

$$s = t, \qquad \mathbf{x} = \mathbf{x}(t, \mathbf{X}). \tag{2}$$

In ALE description, a third configuration is needed to take into account grid points:

$$\begin{aligned} &\mathbf{\Psi} : \Omega_{s',\boldsymbol{\xi}} \to \Omega_{\mathbf{x}}, \\ &\quad (s', \boldsymbol{\xi}) \to (t, \mathbf{x}) = \mathbf{\Psi}(s', \boldsymbol{\xi}). \end{aligned} \tag{3}$$

The law of motion linking both mesh $\boldsymbol{\xi}$ and spatial $\mathbf{x}$ particles in time :

$$s' = t, \qquad \mathbf{x} = \mathbf{x}(t, \boldsymbol{\xi}). \tag{4}$$

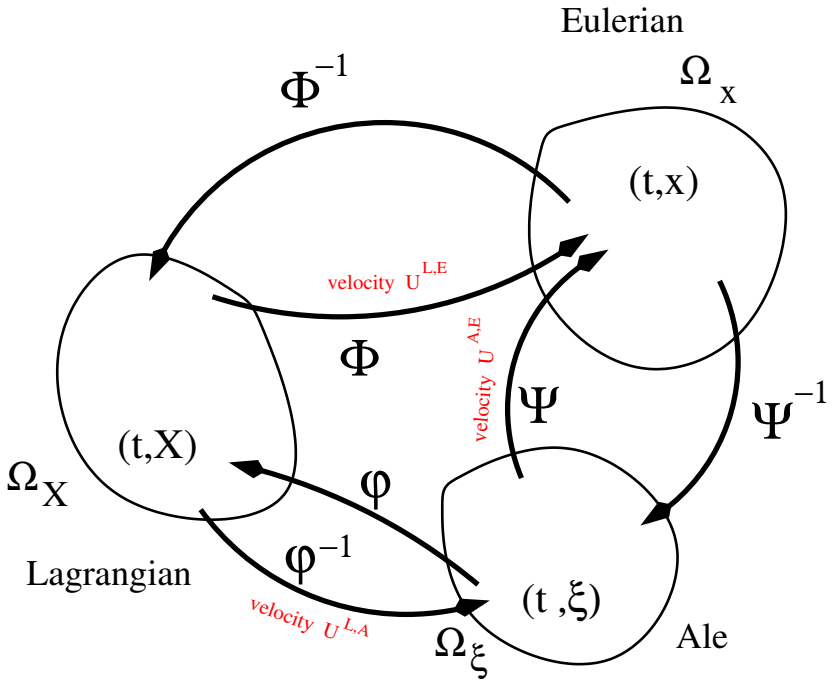

Figure 1: The three canonical configuration for description of (non-relativistic) motion: Lagrangian, Eulerian, ALE (see Figure 2). Maps between initial coordinate systems (Lagrangian), final (Eulerian) and referential (ALE) configurations: we note by $\mathbf{X}$ (resp. $\mathbf{x}$ and $\boldsymbol{\xi}$) the Lagrangian (resp. Eulerian and ALE) coordinates.

Each velocities can be deduced for each law of motion:

- Material velocity associated to the map acting from material (Lagrangian) onto spatial current (Eulerian) configuration (see (2)):

$$\mathbf{U}^{\mathbf{L},\mathbf{E}}(t,\mathbf{X}) = \frac{\partial}{\partial t}\mathbf{x}(t,\mathbf{X})|_{\mathbf{X}} \tag{5}$$

$$= \mathbf{U}^{\mathbf{L},\mathbf{E}}(\Phi^{-1}(t,\mathbf{x})) := \mathbf{U}(t,\mathbf{x}). \tag{6}$$

- ALE velocity associated to the map acting from grid onto spatial current configuration (see (4)):

$$\mathbf{U}^{\mathbf{A},\mathbf{E}}(t,\boldsymbol{\xi}) = \frac{\partial}{\partial t}\mathbf{x}(t,\boldsymbol{\xi})|_{\boldsymbol{\xi}} \tag{7}$$

$$= \mathbf{U}^{\mathbf{A},\mathbf{E}}(\Psi^{-1}(t,\mathbf{x})) := \mathbf{V}(t,\mathbf{x}). \tag{8}$$

Dealing now with the transformation from material to reference frame (see Figure 1):

$$\begin{aligned} \varphi^{-1} : \Omega_{s,\mathbf{X}} &\to \Omega_{\boldsymbol{\xi}}, \\ (s,\mathbf{X}) &\to (t,\boldsymbol{\xi}) = \varphi^{-\mathbf{1}}(s,\mathbf{X}). \end{aligned} \tag{9}$$

In this case, the velocity of material particle in referential mesh is

$$\mathbf{U}^{\mathbf{L},\mathbf{A}}(t,\mathbf{X}) = \frac{\partial}{\partial t}\boldsymbol{\xi}(t,\mathbf{X})|_{\mathbf{X}} \tag{10}$$

$$= \mathbf{U}^{\mathbf{L},\mathbf{A}}((\varphi \circ \Psi^{-1})(t,\mathbf{x})) := \mathbf{W}(t,\mathbf{x}). \tag{11}$$

See for example [18], the relation between velocities (5)(7) (10) obtained by differentiating the identity $\Phi = \Psi \circ \varphi^{-1}$ (see Figure 1) wrt $(t,\mathbf{X})$ variable:

$$\mathbf{U}^{\mathbf{L},\mathbf{E}} = \mathbf{U}^{\mathbf{A},\mathbf{E}} + \frac{\partial \mathbf{x}}{\partial \boldsymbol{\xi}}.\mathbf{U}^{\mathbf{L},\mathbf{A}} \tag{12}$$

the difference between material and mesh velocity see (5)(7) is (in practice) an important variable:

$$\mathbf{c} := \mathbf{U}^{\mathbf{L},\mathbf{E}} - \mathbf{U}^{\mathbf{A},\mathbf{E}} = \frac{\partial \mathbf{x}}{\partial \boldsymbol{\xi}}.\mathbf{U}^{\mathbf{L},\mathbf{A}} \tag{13}$$

$$\mathbf{c} := \mathbf{U} - \mathbf{V} = \frac{\partial \mathbf{x}}{\partial \boldsymbol{\xi}}.\mathbf{W} \tag{14}$$

Note that in the ambient space $I\!R^d$, there are now three alternative to describe a single scalar quantity: $f(t,\mathbf{x}), f^*(t,\boldsymbol{\xi}), f^{**}(t,\mathbf{X})$ depending on the configuration: spatial, referential or material domain. We give now a brief description of useful relationship between time evolution of such quantities.

2.2 Time derivative of punctual values

We give some relation between different time derivatives:

1. Spatial $f(t,\mathbf{x})$ and material $f^{**}(t,\mathbf{X})$, thanks to (1), we have $f^{**}(t,\mathbf{X}) = f(\Phi(t,\mathbf{X}))$, so that by differentiating in $(t,\mathbf{X})$ variable and using (5):

$$\begin{array}{ll} \frac{\partial}{\partial t} f^{**}|_{\mathbf{X}} & = \frac{\partial}{\partial t} f|_{\mathbf{x}} + \frac{\partial}{\partial t}\mathbf{x}.\nabla_{\mathbf{x}} f(t,\mathbf{x}) = \frac{\partial}{\partial t} f|_{\mathbf{x}} + \mathbf{U}(t,\mathbf{x}).\nabla_{\mathbf{x}} f(t,\mathbf{x}) \\ \frac{\partial}{\partial t}(J_{\mathbf{x}\mathbf{X}} f^{**})|_{\mathbf{X}} & = J_{\mathbf{x}\mathbf{X}}\left(\frac{\partial}{\partial t} f|_{\mathbf{x}} + \nabla_{\mathbf{x}}.(f(t,\mathbf{x})\mathbf{U}(t,\mathbf{x}))\right), \quad J_{\mathbf{x}\mathbf{X}} := det\frac{\partial \mathbf{x}}{\partial \mathbf{X}}. \end{array} \tag{15}$$

   First equation in (15) is nothing but the total time derivative (material) ($\frac{d}{dt}(.) := \frac{\partial}{\partial t}(.)|_{\mathbf{X}}$).

2. Referential $f^*(t,\boldsymbol{\xi})$ and material $f^{**}(t,\mathbf{X})$, thanks to (9), we have $f^{**}(t,\mathbf{X}) = f^*(\varphi^{-1}(t,\mathbf{X}))$, so that by differentiating in $(t,\mathbf{X})$ variable and using (10) (13) (14) :

$$\begin{array}{ll} \frac{\partial}{\partial t} f^{**}|_{\mathbf{X}} & = \frac{\partial}{\partial t} f^*|_{\boldsymbol{\xi}} + \frac{\partial}{\partial t}\boldsymbol{\xi}.\nabla_{\boldsymbol{\xi}} f^*(t,\boldsymbol{\xi}) \\ & = \frac{\partial}{\partial t} f^*|_{\boldsymbol{\xi}} + \mathbf{W}(t,\mathbf{x}).\frac{\partial \mathbf{x}}{\partial \boldsymbol{\xi}}\nabla_{\mathbf{x}} f(t,\mathbf{x}) \\ & = \frac{\partial}{\partial t} f^*|_{\boldsymbol{\xi}} + \mathbf{c}(t,\mathbf{x}).\nabla_{\mathbf{x}} f(t,\mathbf{x}) \\ \frac{\partial}{\partial t}(J_{\boldsymbol{\xi}\mathbf{X}} f^{**})|_{\mathbf{X}} & = J_{\boldsymbol{\xi}\mathbf{X}}\left(\frac{\partial}{\partial t} f^*|_{\boldsymbol{\xi}} + \nabla_{\mathbf{x}}.(f(t,\mathbf{x})\mathbf{c}(t,\mathbf{x}))\right), \quad J_{\boldsymbol{\xi}\mathbf{X}} := det\frac{\partial \boldsymbol{\xi}}{\partial \mathbf{X}}. \end{array} \tag{16}$$

3. Spatial $f(t,\mathbf{x})$ and referential $f^*(t,\boldsymbol{\xi})$, thanks to (3), we have $f^*(t,\boldsymbol{\xi}) = f(\Psi(t,\boldsymbol{\xi}))$, so that by differentiating in $(t,\boldsymbol{\xi})$ variable and using (7):

$$\begin{array}{ll} \frac{\partial}{\partial t} f^*|_{\boldsymbol{\xi}} & = \frac{\partial}{\partial t} f|_{\mathbf{x}} + \frac{\partial}{\partial t}\boldsymbol{\xi}.\nabla_{\mathbf{x}} f(t,\mathbf{x}) = \frac{\partial}{\partial t} f|_{\mathbf{x}} + \mathbf{V}(t,\mathbf{x}).\nabla_{\mathbf{x}} f(t,\mathbf{x}) \\ \frac{\partial}{\partial t}(J_{\mathbf{x}\boldsymbol{\xi}} f^*)|_{\boldsymbol{\xi}} & = J_{\mathbf{x}\boldsymbol{\xi}} \left(\frac{\partial}{\partial t} f|_{\mathbf{x}} + \nabla_{\mathbf{x}}.(f(t,\mathbf{x})\mathbf{V}(t,\mathbf{x})) \right), \quad J_{\mathbf{x}\boldsymbol{\xi}} := det \frac{\partial \mathbf{x}}{\partial \boldsymbol{\xi}}. \end{array} \tag{17}$$

All '*' indices are omitted thereafter.

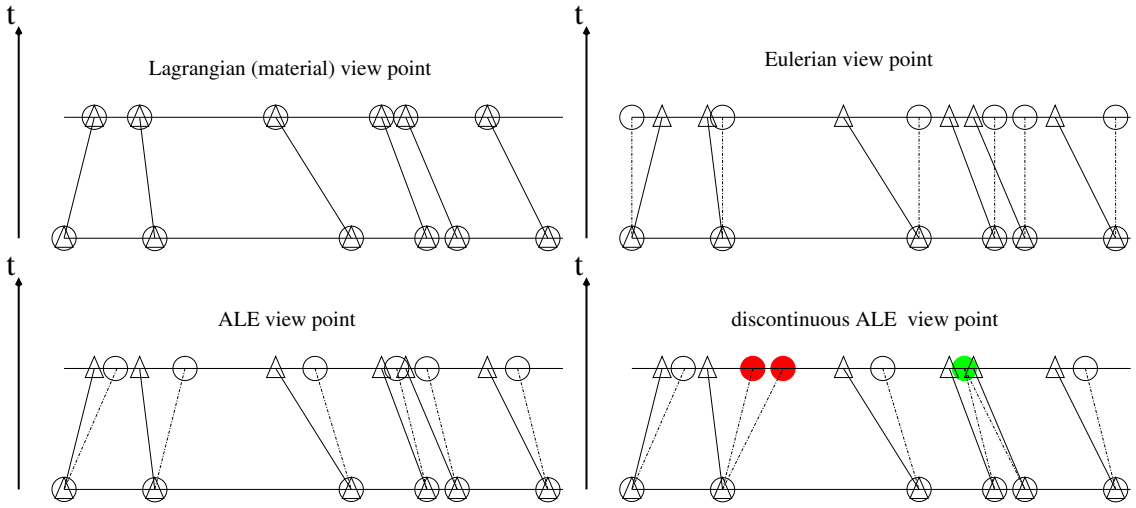

Figure 2: Different descriptions Lagrange, Euler, ALE and associated kinematic
◯ Mesh node -·- mesh motion
△ Material point ——— particle motion
Duplication as well as merging of nodes in mesh update step can be seen as a discretization of a discontinuous ALE kinematic framework (see Figure 4)

We resume the main idea of the paper (Figure 2): we make an analogy that mesh generation result in discretization of computational domain and

mesh h-adaptation result in discretization of discontinuous ALE framework.

2.3 Time derivative of integral spatial quantity

In this case, we essentially recall the Reynolds transport theorem, the control volume evolution for a spatial eulerian quantity $f(t,\mathbf{x})$ over a cell whose boundary points are moving with different velocity depending on description see Figure 3.

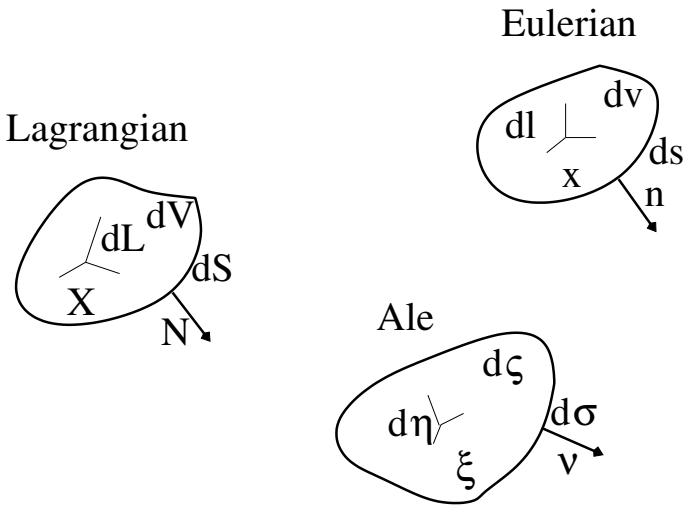

Figure 3: Notation for geometrical information for different configurations

1. material speed (5):

$$\frac{d}{dt}\int_{C^{MAT}(t)} f(t,\mathbf{x})dx = \int_{C^{MAT}(t)} \frac{\partial}{\partial t} f(t,\mathbf{x})dx + \int_{\partial C^{MAT}(t)} f(t,\mathbf{x})\mathbf{U}(t,\mathbf{x}).\mathbf{n}ds \quad (18)$$

2. referential ALE speed (7):

$$\frac{\partial}{\partial t}|_{\boldsymbol{\xi}} \int_{C^{ALE}(t)} f(t,\mathbf{x})dx = \int_{C^{ALE}(t)} \frac{\partial}{\partial t} f(t,\mathbf{x})dx + \int_{\partial C^{ALE}(t)} f(t,\mathbf{x})\mathbf{V}(t,\mathbf{x}).\mathbf{n}ds \quad (19)$$

2.4 System of governing equations

Written over a frame moving with an arbitrary velocity $\mathbf{V}$, integrals forms on a generic cell $C(t)$ of Euler system of gaz dynamics of density ρ, velocity $\mathbf{U}$ and specific total energy E on spatial Eulerian configuration (also called ALE updated form) (see [19][24][14][17][32][18]):

1) Conservation laws in integral forms in ALE configuration for $t \in [t_1, t_2]$:

$$\left\{ \begin{array}{lcl} \frac{\partial}{\partial t}|_{\boldsymbol{\xi}} \int_{C(t)} 1dx - \int_{\partial C(t)} \mathbf{V}.\mathbf{n}ds & = & 0, \text{ (volume)} \\ \frac{\partial}{\partial t}|_{\boldsymbol{\xi}} \int_{C(t)} \rho dx + \int_{\partial C(t)} \rho(\mathbf{U}-\mathbf{V}).\mathbf{n}ds & = & 0, \text{ (mass)} \\ \frac{\partial}{\partial t}|_{\boldsymbol{\xi}} \int_{C(t)} \rho\mathbf{U}dx + \int_{\partial C(t)} ((\rho\mathbf{U}\otimes(\mathbf{U}-\mathbf{V}))\mathbf{n} + P\mathbf{n})ds & = & 0, \text{ (momentum)} \\ \frac{\partial}{\partial t}|_{\boldsymbol{\xi}} \int_{C(t)} \rho E dx + \int_{\partial C(t)} (\rho E(\mathbf{U}-\mathbf{V}) + P\mathbf{U}).\mathbf{n}ds & = & 0, \text{ (total energy)} \\ \text{where pressure } P(\rho,\epsilon),\ \epsilon \textit{ internal energy}, & & \\ \epsilon = E - \frac{1}{2}|\mathbf{U}|^2 \ + \textit{ Entropy}. & & \end{array} \right. \quad (20)$$

2) Kinematic equation for ALE configuration (see (7)(8)) in ponctual trajectory form:

$$\left\{ \begin{array}{l} \frac{d}{dt}\mathbf{x} = \mathbf{V}(t,\mathbf{x}) \\ x(t=t_1) = x^* \text{ given} \end{array} \right. \tag{21}$$

x^* (seen as a label) is defined on boundary cell in practice because of flux are defined on $\partial C(t)$ in (20).

Remark 1

- *The system (20) is expressed with Eulerian variable coordinate. This also called update ALE form (U-ALE see [6] [5]).*
- *In the following, we adopt an operator splitting strategy. Practically, the velocity* $\mathbf{V}$ *is decomposed in physical fluid speed and a (relative) grid speed:* $\mathbf{V} = \mathbf{U} - \mathbf{V^{Grid}}$*, and the resulting system is solved by a splitting separating fluids and grid contributions (S-U-ALE see also [5]).*

In a first purely hydrodynamical step $\mathbf{V} = \mathbf{U}$, only pressure appears in physical thermodynamical flux. If we note by $C^{MAT}(t)$, the moving material cell associated to kinematic equation (5)(6), the evolution of individual point is given by an approximate multi-dimensional Riemann solver associated to the hydrodynamic part. In the context of centered finite volume scheme see [17, 12, 32, 13]:

$$\left\{ \begin{array}{l} \frac{\partial}{\partial t}\int_{C^{MAT}(t)} 1dx - \int_{\partial C^{MAT}(t)} \mathbf{U}.\mathbf{n}ds = 0, \\ \frac{\partial}{\partial t}\int_{C^{MAT}(t)} \rho dx = 0, \\ \frac{\partial}{\partial t}\int_{C^{MAT}(t)} \rho\mathbf{U}dx + \int_{\partial C^{MAT}(t)} P\mathbf{n}ds = 0, \\ \frac{\partial}{\partial t}\int_{C^{MAT}(t)} \rho E dx + \int_{\partial C^{MAT}(t)} P\mathbf{U}.\mathbf{n}ds = 0. \end{array} \right. \tag{22}$$

We recall that (22) is the updated-Lagrangian form of Gaz Dynamics Euler system, where the spatial quantities are written with Eulerian coordinates like (20), it correspond to local differential operator at point (t,$\mathbf{x}$) ($\mathbf{x}$ Eulerian coordinate) see (15). The second part of the splitting $\mathbf{V} = -\mathbf{V}^{Grid}$ gives a system of conservative advection equations. Here, the moving cell is noted $C^{ADV}(t)$:

$$\left\{ \begin{array}{ll} \frac{\partial}{\partial t}\int_{C^{ADV}(t)} 1dx + \int_{\partial C^{ADV}(t)} 1\mathbf{V}^{Grid}.\mathbf{n}ds = 0, & (\text{ GCL}) \\ \frac{\partial}{\partial t}\int_{C^{ADV}(t)} \rho dx + \int_{\partial C^{ADV}(t)} \rho\mathbf{V}^{Grid}.\mathbf{n}ds = 0, & \\ \frac{\partial}{\partial t}\int_{C^{ADV}(t)} \rho\mathbf{U}dx + \int_{\partial C^{ADV}(t)} (\rho\mathbf{U})\mathbf{V}^{Grid}.\mathbf{n}ds = 0, & \\ \frac{\partial}{\partial t}\int_{C^{ADV}(t)} \rho E dx + \int_{\partial C^{ADV}(t)} \rho E\mathbf{V}^{Grid}.\mathbf{n}ds = 0. & \end{array} \right. \tag{23}$$

As a consequence of the splitting, the kinematic equation (21) of Lagrangian hydrodynamic part (22) in (20) is:

$$\frac{d}{dt}\mathbf{x} = \mathbf{U}(t,\mathbf{x}) \tag{24}$$

while kinematic equation (21) for advection part (23) of (20) is :

$$\frac{d}{dt}\mathbf{x} = -\mathbf{V}^{Grid}(t,\mathbf{x}). \tag{25}$$

In the following, we discuss about the **smoothness** of the arbitrary mesh velocity (25) while looking at exact discretisation of Geometrical Conservation Law (GCL equation see (23)).

3 On existence of discontinuous mesh velocity for the modeling of h-adaptation and reconnection

We emphasize that is not the purpose of this article to have a rigorous mathematical framework. However, it is striking similarities with concepts of functional analysis: BV space to model fields with reasonable discontinuities and Hodge decomposition for the effects related to the physics of rotation and translation. This section is essentially devoted to give some kind of justification of a discontinuous frame to deal with some mesh adaptation with reconnection. More precisely, we are interested **only** on the *existence* of such discontinuous behavior.

For the definition of functional space see for example [11, 9, 36, 29, 3]

3.1 Functional space for transport equation

3.1.1 Definition and basics

We consider that Ω is an open, bounded, connected Lipschitz domain.

- $C_0^1(\Omega)$: the space of C^1 function with compact support in Ω.
- $BUC(\Omega)$: the space of bounded and uniformly continuous functions on Ω.
- $\mathbf{f}$ is $\mathbf{k}$-Lipschitz on Ω:

$$\forall \mathbf{x}, \mathbf{y} \in \Omega, \quad \|\mathbf{f}(\mathbf{x}) - \mathbf{f}(\mathbf{y})\| \leq \mathbf{k}\|\mathbf{x} - \mathbf{y}\| \tag{26}$$

- $L^p(\Omega)$: the Lebesgue space of function : dx is the Lebesgue measure, f in $L^p(\Omega)$ if

  a) $1 \leq p < \infty$

$$|f|_p := \left(\int_\Omega |f|^p dx \right)^{\frac{1}{p}} < +\infty \tag{27}$$

  b) $p = \infty$

$$|f|_\infty := \inf \left\{ K \in I\!R^+ \ ; \ |f| \leq K \ \ a.e. \right\} < +\infty \tag{28}$$

- $W^{1,p}(\Omega)$: the Sobolev space of function: $f \text{ in } W^{1,p}(\Omega)$ if $f \text{ in } L^p(\Omega)$ and all distributional partial derivatives $\frac{\partial f}{\partial x_i}$ are still in $L^p(\Omega)$.
  $W^{1,\infty}(\Omega)$ is the space of function f in $L^\infty(\Omega)$ such that $\exists K > 0$

$$|f(x) - f(y)| \leq K|x - y|, \qquad a.e.\ x, y \in \Omega. \tag{29}$$

- $BV(\Omega)$: the space of function f in $L^1(\Omega)$ such that:

$$TV(f) := \sup \left\{ \int_\Omega f \nabla.\mathbf{g} dx \ ; \ \mathbf{g} \text{ in } (C_0^1(\Omega))^d; |\mathbf{g}|_\infty \leq 1 \right\} < +\infty \tag{30}$$

  The analog to vectorial function : $\boldsymbol{f} \text{in} (BV(\Omega))^d$ is such that $\boldsymbol{f}$ in $(L^1(\Omega))^d$ and:

$$TV(\boldsymbol{f}) := \sup \left\{ \sum_{j=1,d} \int_\Omega f_j \nabla.\mathbf{g_j} dx \ ; \ \mathbf{g_j} \text{ in } (C_0^1(\Omega))^d; |\mathbf{g_j}|_\infty \leq 1 \right\} < +\infty \tag{31}$$

3.1.2 Some properties / Characterization

For the modelization of discontinuous field, Sobolev space are too restrictive (see e.g. [2]) because they do not accept indicator/Heaviside functions, $L^p(\Omega)$ contains discontinuities that are too pathological, beside BV space contains function having discontinuity along or across curves, moreover it posses many practical useful characterizations.

- Let K be smooth compact, $K \subset \Omega$, and χ_K the associated characteristic function, then $\chi_K \notin W^{1,1}(\Omega)$ but $\chi_K \text{ in } BV(\Omega)$.

- $f \text{ in } BV(\Omega)$, the distributional gradient Df is a finite measure, more precisely, Ambrosio see [2][3]:

  - the distributional gradient of function $\mathbf{f} \text{ in } (BV(\Omega))^d$ is decomposed in regular and singular part:

$$D\mathbf{f} = D^a\mathbf{f} + D^s\mathbf{f} = \nabla\mathbf{f} + (\mathbf{J}_f + \mathbf{C}_f) \tag{32}$$

    1. $\nabla\mathbf{f} \text{in} (L^1(\Omega))^d$ is the Radon-Nikodym derivative of $\mathbf{f}$ with respect to Lebesgue measure dx.
    2. $\mathbf{J}_f = (\mathbf{f}^+ - \mathbf{f}^-) \otimes \mathbf{n}_f \mathcal{H}^{d-1}_{|S_f}$ the jump part, with $\mathcal{H}^{d-1}$ the (d-1)-dimensional Hausdorff measure, S_f is the complementary set of Lebesgue points.
    3. $\mathbf{C}_f$ the Cantor part of the measure.

    $SBV(\Omega)$ space is defined by function $f \text{ in } BV(\Omega)$ with $C_f = \emptyset$.
  - the distributional divergence of a vectorial function $\mathbf{f} \text{ in } (BV(\Omega))^d$:

$$D.\mathbf{f} = \sum_i D_i^a f_i + D^S\mathbf{f} \tag{33}$$

3.2 From continuous to discontinuous kinematic speed

In this part, we give some formal concepts that permit to take into account some mesh connectivity modification in advection part of ALE equations (22)(24) (23)(25).

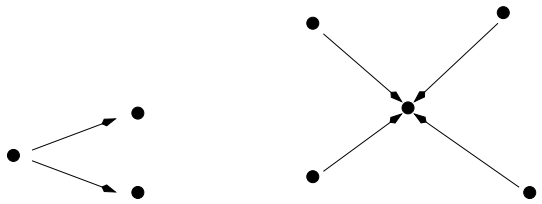

Figure 4: Modeling of duplication (left) and collapse (right) of nodes using discontinuous kinematic velocity

We recall a general theorem of continuum mechanics:

Theorem 1 *Cauchy-Lipschitz*
If the speed $\mathbf{V}^{Grid}(t,\mathbf{x})$ *in (25) is* $(BUC([0,T];\Omega))^d$ *(or Lipschitz), then ALE framework (21)(20) (23) (25) discretize a* **homeomorphic map** *(bijective and bi-continuous).*

Remark 2 *Lagrangian sliding for (22) is not permitted here because of tangential discontinuity in velocity (unless piecewise regularity is replaced by uniform regularity).*

Focusing on advection kinematic equation (25), a direct consequence of these two properties are the two following drawbacks:

- Refinement by

$$\text{vertex} \quad \text{duplication} \tag{34}$$

  is not allowed due to injection of the mapping.

- Coarsening by

$$\text{vertices} \quad \text{collapsing} \tag{35}$$

  is not permitted due to continuity of the mapping.

Hence, the regularity of $\mathbf{V}^{\mathbf{Grid}}(\mathbf{t},\mathbf{x})$ impose that mesh connectivity **can not change**. As a corollary, we have:

Remark 3 *The mesh adaptation within the meaning of (34) (35) cannot be modelized by continuous kinematic speed.*

Lemma 1
A necessary condition to obtain (34) (35) is that the kinematic speed must be **discontinuous** *in space.*

Remark 4 *We are only interested in the* **existence** *of such discontinuous vector field, we do not look for uniqueness. Indeed a strategy to build an optimal "arbitrary discontinuous field" is unreachable, even the (arbitrary) continuous framework is always an open problem. ALE strategy is still highly problem dependent in practice.*

We assume now that the velocity for kinematic advection part can be splitted into a regular (continuous) and non regular (discontinuous) part :

$$\mathbf{V}^{Grid} := \mathbf{V}^{C,Grid} + \mathbf{V}^{D,Grid}. \tag{36}$$

The discontinuous part $\mathbf{V}^{D,Grid}$ of velocity will enable us to take into account mesh connectivity modification (h-adaptation). The continuous part $\mathbf{V}^{C,Grid}$ only deal with mesh modifications keeping the same connectivity (r-adaptation). We consider the equations (20) on an open bounded domain $\Omega \subset I\!R^d$ with Lipschitz boundary. In a finite volume context, we will ask to our extended discontinuous kinematic equation to fulfill the following properties:

1. extension of existing ALE frame for mesh (r,h)-adaptation. The existing Lagrange and rezone/remap phase is naturally enhanced (see [27]) by dynamical topological mesh modification:

$$\begin{cases} \bullet \text{ mesh refinement} \\ \bullet \text{ mesh coarsening} \\ \bullet \text{ generalization of edge swapping to polygons} \\ \bullet \text{ mesh sliding} \end{cases} \tag{37}$$

2. mathematical link for local (r,h)-adaptation on arbitrary polygonal meshes, the h-adaption part must deal with theses hypothesis:

   - Locality
     Find a local generic patch that fulfill any of (37) operation:

     $$\mathbf{V}^{D,Grid}(t,.) \text{ in } (L^\infty(\Omega))^d \tag{38}$$

     $\Rightarrow$ this CFL gives an automatic **locality constraint on remeshing tools**.

   - Physically relevant
     We look at general flows consistency constituted by ***translational*** **and** ***rotational*** **effects**:

     $$\mathbf{V}^{D,Grid}(t,.) = \mathbf{V}^{D,Grid,Tra}(t,.) + \mathbf{V}^{D,Grid,Rot}(t,.) \tag{39}$$

- Generic connectivity
  Cell topology and mesh connectivity are *unknown*, and must be able to adapt itself on local flows (CFL+convexity), here:

  no -a priory- connectivity is imposed to the mesh. (40)

  To adopt a different strategy see ReALE [30] for Voronoy kind of polygonal meshes and a dual approach [10, 1, 7, 16] that impose Delaunay simplicial meshes.

3. We must keep in mind that any new local (r,h)-adaptation must be done under the constraint to exactly solve the DGCL (Discrete Geometric Conservation Laws, first equation of (23) integrated in time):

   - exact DGCL : Let K be a cell or an union of cell C_i see Figure 11 and 12:

$$\int_{K^{n+1}} 1dx = \int_{K^n} 1dx + \int_{t^n}^{t^{n+1}} \left(\int_{\partial K^q} \mathbf{V}^{Grid}(t,x).\mathbf{n}(t,x)ds \right) dt. \quad (41)$$

   - Robust and fast
     No exact polygon/polygon mesh intersection (unless multi-material interface is present).

In the following, we assume the hypothesis:

- Set regularity: Ω is an open bounded set with Lipschitz boundary.
- Functional space: $\mathbf{V}^{D,Grid}(t,.)$ in $L^1(\Omega) \cap L^\infty(\Omega) \cap SBV(\Omega)$
- Growing condition:

$$\nabla.\mathbf{V}^{D,Grid}(t,.) \text{ in } L^\infty(\Omega) \quad (42)$$

  meaning that patch volume of K in (41) stay bounded at each time step.

Theorem 2 *Hodge Decomposition*
It exists a potential vector $\boldsymbol{A}$ *and a potential scalar f such that:*

$$\mathbf{V}^{D,Grid} = \boldsymbol{rotA} - \boldsymbol{\nabla} f. \quad (43)$$

Remark 5 *The vectorial decomposition (43) give a natural modeling of each required properties in (39).*

- $\boldsymbol{rotA}$ *for rotational aspect of the flow.*
- $\boldsymbol{\nabla} f$ *for translational effects.*

As a corollary, it exists a potential vector and a matrix $M \in I\!R^{d\times d}$ such that, assume that $\mathbf{V}^{D,Grid}(t,.)$ in $L^1(\Omega) \cap L^\infty(\Omega) \cap SBV(\Omega)$

Lemma 2

$$\mathbf{V}^{D,Grid} = \boldsymbol{rot}\boldsymbol{A} + \boldsymbol{\nabla}.M \tag{44}$$

Remark 6 *the special structure of matrix M enable to take into account*

- *isotropic translational effects when $M = f\ I$ (diagonal matrix for scalar f) see (43).*
- *anisotropic translational effects when M is a full matrix or*

$$\begin{pmatrix} a & 0 \\ 0 & b \end{pmatrix}, a \neq b \tag{45}$$

- *we recall that we are only interested on existence for (43)(44).*
- *the regularity of potentials functions in (43) depends on the boundary condition for $\mathbf{V}^{D,Grid}(t,.)$ because of the pde constrain:*

$$\begin{array}{lrcll} \text{pde} & -\Delta f & = & \nabla.\mathbf{V}^{D,Grid} & in\ \Omega, \\ \text{boundary condition} & f & = & ? \quad on\ \partial\Omega. & \end{array} \tag{46}$$

Where the (continuous) unspecified boundary condition (46) depends on the (discretized) atomic mesh operation we consider (refinement/coarsening or swapping, see paragraph (3.3.3)). In terms of PDE, the flow acting on $\mathbf{V}^{D,Grid}$ corresponds to a linear multi-dimensional advection with **discontinuous** coefficients. These kind of equations have been studied:

Theorem 3 *[8, 9, 36] If the velocity* $\mathbf{a}(t,\mathbf{x})$ in $L^1_{loc}((0,+\infty);L^\infty(I\!R^d))^d$,

$$\partial_t u + \mathbf{a}(t,\mathbf{x}).\nabla u = 0. \tag{47}$$

is well posed if the sufficient condition OSLC (uniqueness of Filipov characteristics).

$$(\mathbf{a}(t,\mathbf{x}) - \mathbf{a}(t,\mathbf{y}), \mathbf{x}-\mathbf{y}) \leq \alpha(t)|\mathbf{x}-\mathbf{y}|^2, \qquad \alpha(t) \geq 0, \alpha \text{ in } L^1(0,+\infty). \tag{48}$$

As a consequence compressives discontinuities are well posed while rarefaction corresponds to non uniqueness.

Moreover, we recall (see [9]) that in the case of piecewise regular velocity across a smooth hypersurface $\mathbf{S}$, the directional jump depends upon hypothesis on $\mathbf{a}$:

- Tangential to $\mathbf{S}$, it corresponds to absolute continuity of divergence velocity ($\nabla.\mathbf{a}$ absolutely continuous cf [9]).
- Normal to $\mathbf{S}$ corresponds to OSLC (48).

Remark 7 *We recall that evolution by* **level-sets** *to change the co-dimension of a manifold gives raise naturally to this kind of discontinuous PDE see [22, 21], and Figure 5.*

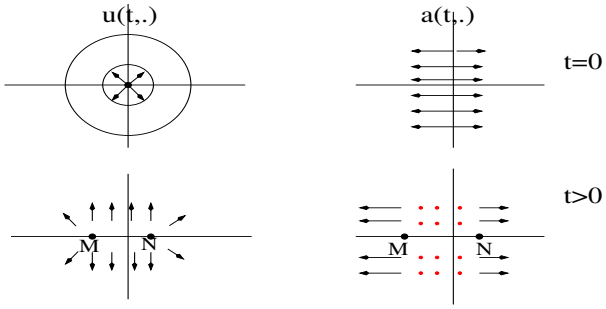

Figure 5: Evolving co-dimension of geometrical objects see [22, 21]. If u_0 is a distance to the origin (up Left) and the initial velocity field $\mathbf{a}$ (up right) then solution of $u_t + \mathbf{a}.\nabla u = 0$ at time t is the distance to the edge defined by $[M(t), N(t)]$.

To summarize this part, we have introduce a discontinuous framework that give a natural way to modelize (34) (35). Comparing to Cauchy-Lipschitz, our assumption of weaker regularity on mesh velocity appears to be *necessary* to take into account dynamical topological mesh change also called h-adaptation.

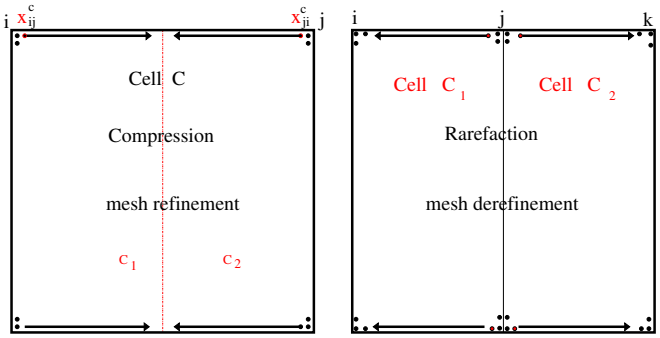

Figure 6: Mesh modification seen as discontinuous grid velocity. Refinement (Left) corresponds to node colliding and transversal reconnection. Coarsening (Right) corresponds to node duplication and opposite reconnection. At first sight this corresponds exactly to the opposite situation of the Figure 4 but this is due to the opposite sign in (25).

3.3 Local mesh patch for discretization of discontinuous kinematic and DGCL

3.3.1 Notations

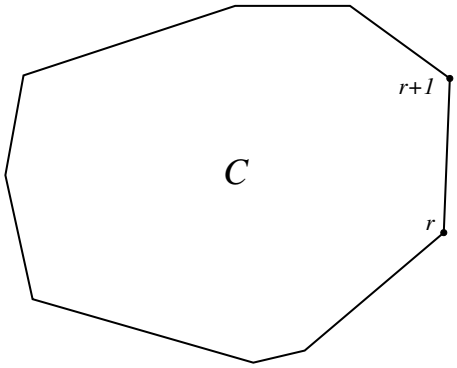

Figure 7: Notation for cell item

- Cell items. Let $N(C)$ the set of nodes belonging to polygonal cell C, we note:

$$NbNode(C) = card(N(C)) \text{ the number of nodes in cell C.} \tag{49}$$

3.3.2 Description of semi conformal object

In [26], we have proposed a preliminary way to recover and extend the philosophy for quadrangle cells toward arbitrary polygons of ALE-AMR (quad-tree based) developed in [4, 34, 35, 28]. It turns out that in our framework, semi-conformity of the mesh is very natural and is a central tool to describe anisotropic adaptation for non simplicial meshes, consider as an example the layer h-adaptation in Figure 6 or in numerical section 4.
Description of local semi-conformity for polygonal cells:

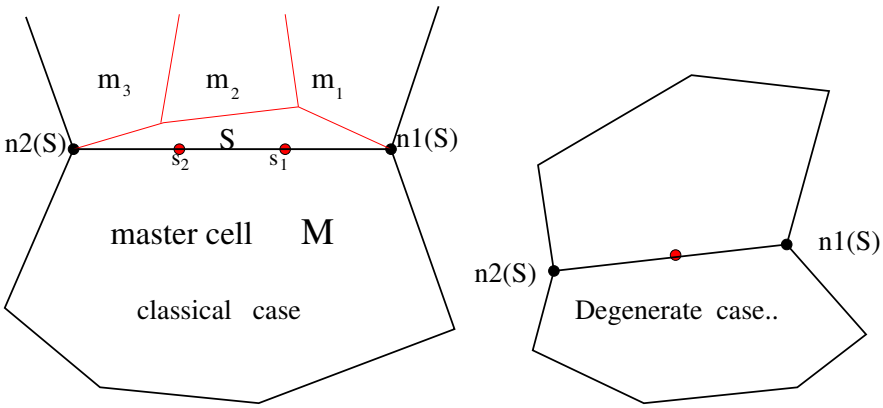

Figure 8: A welding line S of size two, the master cell M, master nodes (n1(S),n2(S)), semi-slaves nodes (S_1,S_2) and cells (m_1,m_2,m_3)

Definition 1 *welding line*
The topology of a welding line S is an union of straight edges, and it is one-sided non conforming (semi conforming).

1. Two master nodes n1(S), n2(S), **semi-slaves** nodes S_i.
2. The master cell M and semi slaves cells m_i.
3. It's level defined by : l(S)=min(l(n1(S)),l(n2(S))) (computed recursively).
4. *Geometrical constraint: We accept it only if master/secondary cells are* **convex between n1(S), n2(S)** *(locally flat is permitted) see Figure 8, hence semi conformity is a relaxed form of non conformity (but contains it).*
5. *A boolean flag that take into account this semi-conformal representation (if not activated, the node are free and the mesh is locally polygonal and unstructured).*

The depth of the mesh $\mathcal{M}$ is then defined by: $\min_{S\in\mathcal{M}}$ l(S).

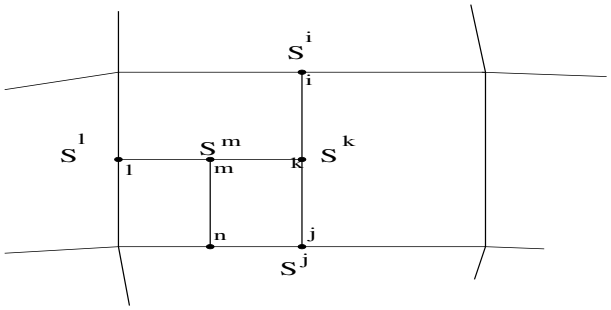

Figure 9: The level of nodes and different imbricated welding lines

There are some practical aspects:

1. arbitrary nested levels are possible,
2. no octree point of view,
3. data structure is an hybrid representation of unstructured meshes and semi-conformity (see Definition 1 above), this kind of storage is useful when dealing with continuous rezoning and remapping.
   - continuous rezoning must take into account semi-conformal aspect of the mesh.
   - remapping only deal with the (unstructured) polygonal topology of the mesh, each edge (conformal or semi-slave) displacement induce his own fluxed volume.

Definition 2 *Sliding edge*
A sliding edge (see Figure 10) is an edge that belongs to two different adjacent welding lines see Definition 1 (see Figure 8):

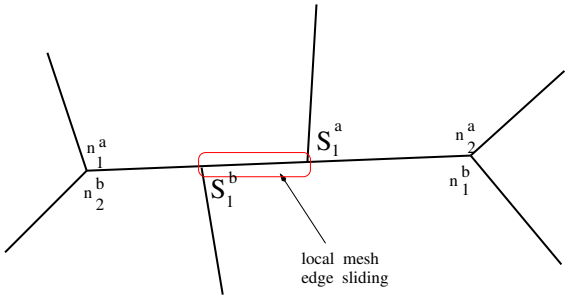

Figure 10: A mesh edge sliding is an edge that simultaneously belongs to two welding lines.

In the design of an exact DGCL scheme for (41), we begin to define the central patch $\mathcal{P}(\mathrm{e})$ constituted by an edge surrounded by its neighboring cells, there are two situations depending on the nature of the edge:

1. Case of conformal edge (see Figure 11):

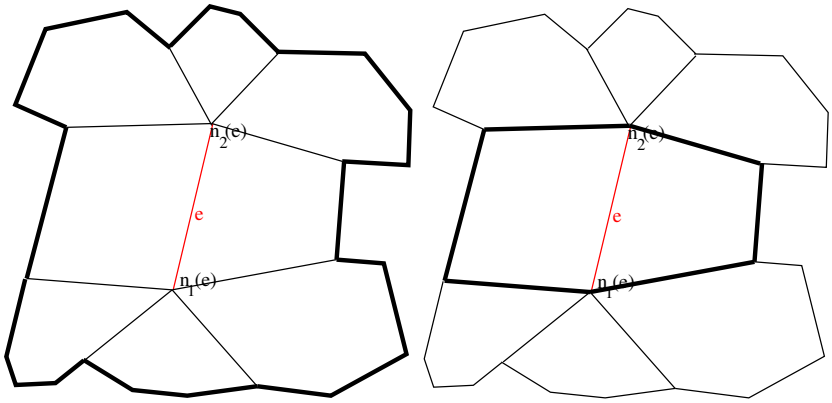

Figure 11: Generic patch $\mathcal{P}(\mathrm{e})$: cell-edge stencil for conformal edge. Left: all cell containing at least a node of edge e. Right: only the two adjacent cells. Solid lines are pieces of boundary cells for each neighborhood.

2. Case of semi conformal edge (see Figure 12):

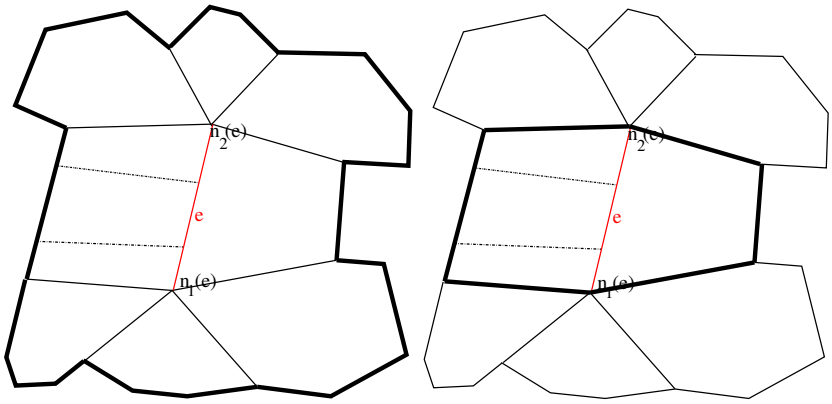

Figure 12: Generic patch $\mathcal{P}(\mathrm{e})$: cell-edge stencil for semi-conformal edge. Left: all cell containing at least a node extremity or semi-slave node of edge e. Right: only the master and semi-slaves cells. Solid lines are pieces of boundary cells for each neighborhood.

To solve our constraints (37) and fulfill locality hypothesis (38), we need to define two sets for each conformal or semi-conformal edge:

1. $\mathcal{P}^e$: Conformal case (see Figure 11):

$$\begin{array}{l} \mathcal{P}^e(\mathrm{e}) = \{C; \mathrm{e} \subset C\}\,, \\ \mathcal{P}^C(\mathrm{e}) = \{C; \mathrm{n}_1(\mathrm{e}) \ \text{ or } \mathrm{n}_2(\mathrm{e}) \subset C\}\,. \end{array} \tag{50}$$

2. $\mathcal{P}^e$: Semi-conformal case (see Figure 12):

$$\begin{array}{l} \mathcal{P}^e(\mathrm{e}) = \{C; \mathrm{e} \subset C \ \text{ or } \exists i, \mathbf{S_i} \subset C\}\,, \\ \mathcal{P}^C(\mathrm{e}) = \{C; \mathrm{n}_1(\mathrm{e}) \ \text{ or } \mathrm{n}_2(\mathrm{e}) \subset C \ \text{ or } \exists i, \mathbf{S_i} \subset C\}\,. \end{array} \tag{51}$$

3. We can define the exterior boundary of each of these neighborhoods $\mathcal{P}(\mathrm{e})$:

$$\mathcal{B}(\mathcal{P}) = \{x \in \mathrm{e}'/\mathrm{e}' \in \mathcal{P}(\mathrm{e}) \ \text{ is an exterior edge}\} \tag{52}$$

   $\mathcal{B}(\mathcal{P})$ corresponds for each set $\mathcal{P}^e(e)$ (two adjacent cells) and $\mathcal{P}^C(e)$ (all cells containing any of two endpoints) to bold lines in Figure 11 and 12.

In the following, to satisfy the locality hypothesis (38), we assume that:

Hypothesis 1 *$\mathcal{B}(\mathcal{P})$ (solid lines in Figure 11 and 12) is union of edges (globally Lipschitz curve) supposed to be **fixed** with respect to generic edge e.*

$$\textit{Local patch volume preservation,} \qquad \frac{d}{dt}|\mathcal{P}(\mathrm{e})| = 0. \tag{53}$$

3.3.3 Refinement/Coarsening/Swapping and Reconnection

This step is constituted by two stages:

1) add, remove or transform edges or vertices.

2) perform underlying reconnections to obtain locally new cell configuration.

We consider separately the refinement and coarsening:

Refinement :

A local cell by cell approach see also [34, 35]:
We collect nodal informations (geometrical and physical) that take into account mesh regularity and flow singularities using local gradient or hessian estimates.
Loop on nodes n:

1. Geometrical criteria around n: $Q_n^{GEOM}\left(\frac{\min_C Area(C)}{\max(\max_C Area(C), |\min_C Area(C)|)}\right)$
2. Physical criteria around n: Q_n^{PHYS} $(w(x) = 1 + ||\nabla^2 \rho_n||_2^2)$.

We tag a node as "refinement" if we have both:

$$\left\{ \begin{array}{l} Q_n^{GEOM} > Q^{GEOM,ref} \ \textbf{and} \\ Q_n^{PHYS} > Q^{PHYS,ref} \ \text{ and all } \textbf{local extrema} \text{ of } w(x). \end{array} \right. \tag{54}$$

Loop on cells C:
We define two numbers:

1. $Nb^{ref}(C)$ all the nodes marked as "refinement".
2. $Nb^{cons}(C)$ all of the **consecutive** marked nodes.

Reconnection by local topology study (short range)

1. *Anisotropic refinement (1D)* : For the two consecutive nodes, if the criteria values are **nearly equal**,

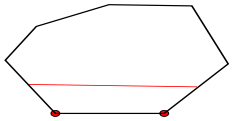

Figure 13: We link the previous mid edge with the next mid edge.

2. *Quasi one-dimensional (uni-directional) refinement (Q1D)* : For the two consecutive nodes, if the criteria values are **different**,

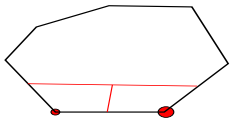

Figure 14: We link the previous mid edge with the next mid edge and then mid point of the new edge to mid edge of current edge.

3. *Isotropic refinement*: If we have $Nb^{ref}(C) > \frac{NbNode(C)}{2}$, and $Nb^{ref}(C) > 4, NbNode(C) > 2$

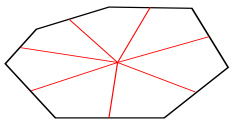

Figure 15: Each mid edge is linked to a center point of cell C.

In any situation above (13), (14) and (15) the computation of new conservative quantities is straightforward for a first order scheme, we just put the coarse value on each of the new sub cells.

Coarsening :

Loop on nodes n:

1. Geometrical criteria around n: $Q_n^{GEOM}\left(\frac{\min_C Area(C)}{\max(\max_C Area(C), |\min_C Area(C)|)}\right)$.
2. Physical criteria around n: Q_n^{PHYS} (w(x)=1+ $||\nabla^2\rho_n||_2^2$), and Local bad CFL.

We mark a node coarsened if we have both $Q_n^{GEOM} < Q^{GEOM,coarse}$ and $Q_n^{PHYS} < Q^{PHYS,coarse}$.
We have two possible choice:

1. If Q_{n1}^{PHYS} and Q_{n2}^{PHYS} **are nearly equal** : Clear edges such their two end points are tagged "coarse": cell aggregation (Full edge Coarsening case).

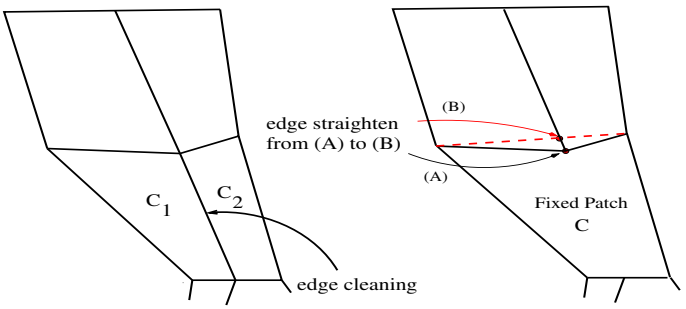

Figure 16: Edge deleting: In case of convex cell enforcement, a straighten edge approach may be used.

The new centered conservatives values are obtained by:

(a) Compute the total volume and mass of **fixed patch** $C = C_1 \cup C_2$, and density redistribution (cte) inside the new cell.
(b) Compute intersection between welding line and the canceled edge.
(c) Compute new fluxed quantities by self intersection.
(d) The degenerate welding lines (see Figure 8) are cleared (vertex cleaning). Note that layer by layer coarsening is recovered if flow possess symmetries.

2. If Q_{n1}^{PHYS} and Q_{n2}^{PHYS} **are different**, an edge to vertex transformation is performed:

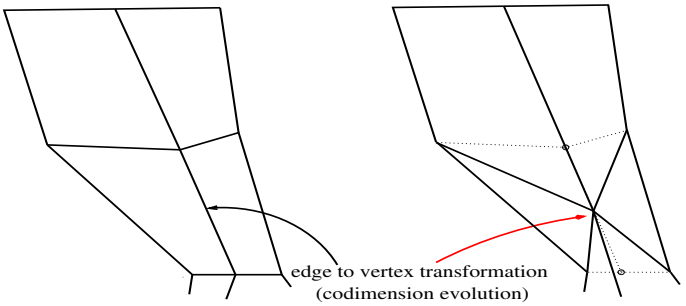

Figure 17: Edge to vertex transformation

Volume fluxing is obviously computed by classical local flux scheme (endpoint displacement), it involves all the cells in the patch (in case of any of initial triangular adjacent cell, his deletion is done at the end of the remap).

Extended swapping :

In this part we introduce a discontinuous transformation of boundary of two adjacent arbitrary cells. This is a natural extension of diagonal edge swapping from simplices to polygonal cells.
Diagonal flipping (Figure 18) between two adjacent simplices is performed to enhance some criteria:

- geometric: mesh quality measure (e.g. Delaunay criteria) of a cell.
- stability: local CFL, we recall that stability criteria for explicit finite volume method is proportional to:

$$J^{CFL}(C) := \frac{|C|}{\sum_e |e|}. \tag{55}$$

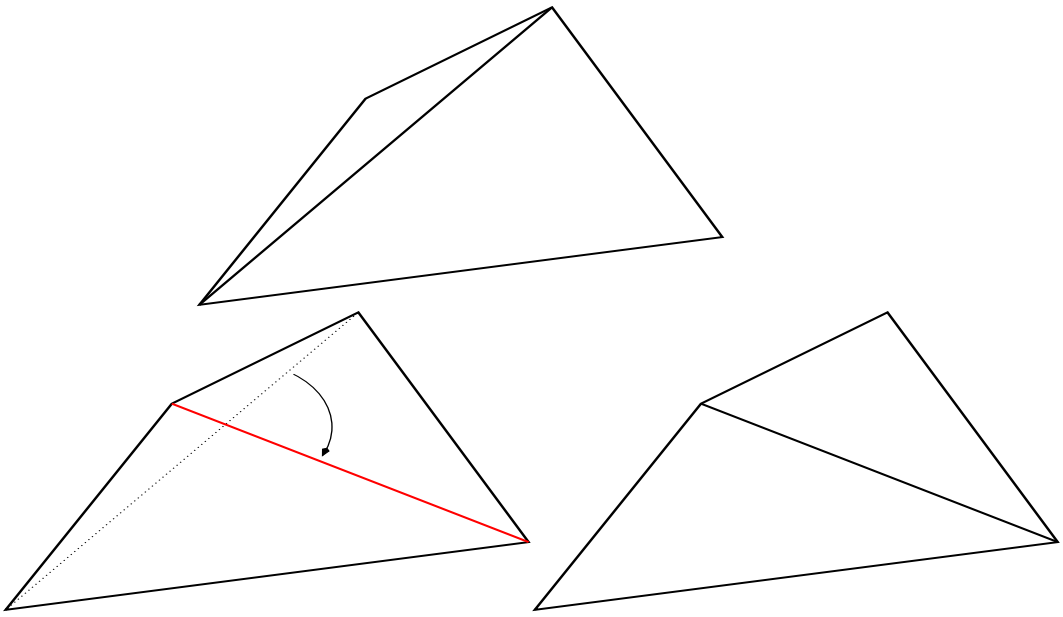

Figure 18: Triangular swapping from old (black doted line) to new (red) configurations

Proposition 1 *Continuous Generic Extension of Edge Swapping*
Consider a two adjacent cell patch (see (11) (12)), C_1 and C_2. Consider a cell measure quality J(C) (e.g. the CFL measure (55) of a cell). We

consider the problem of finding a new path e^* linking two points of $\mathcal{B}(\mathcal{P}^e)$ solution of continuous optimization problem:

$$\max_{e'} \min(J(C_1'), J(C_2')) \tag{56}$$

where C_i' are virtual cells created by virtual movement of edge $\mathbf{e}'$. For polygonal cells, such a continuous problem is approximated by finite tests on successive configurations (see Figure 19). Candidate path e' is a straight segment joining two points, each of them being either a (existing) node or a mid-edge point.

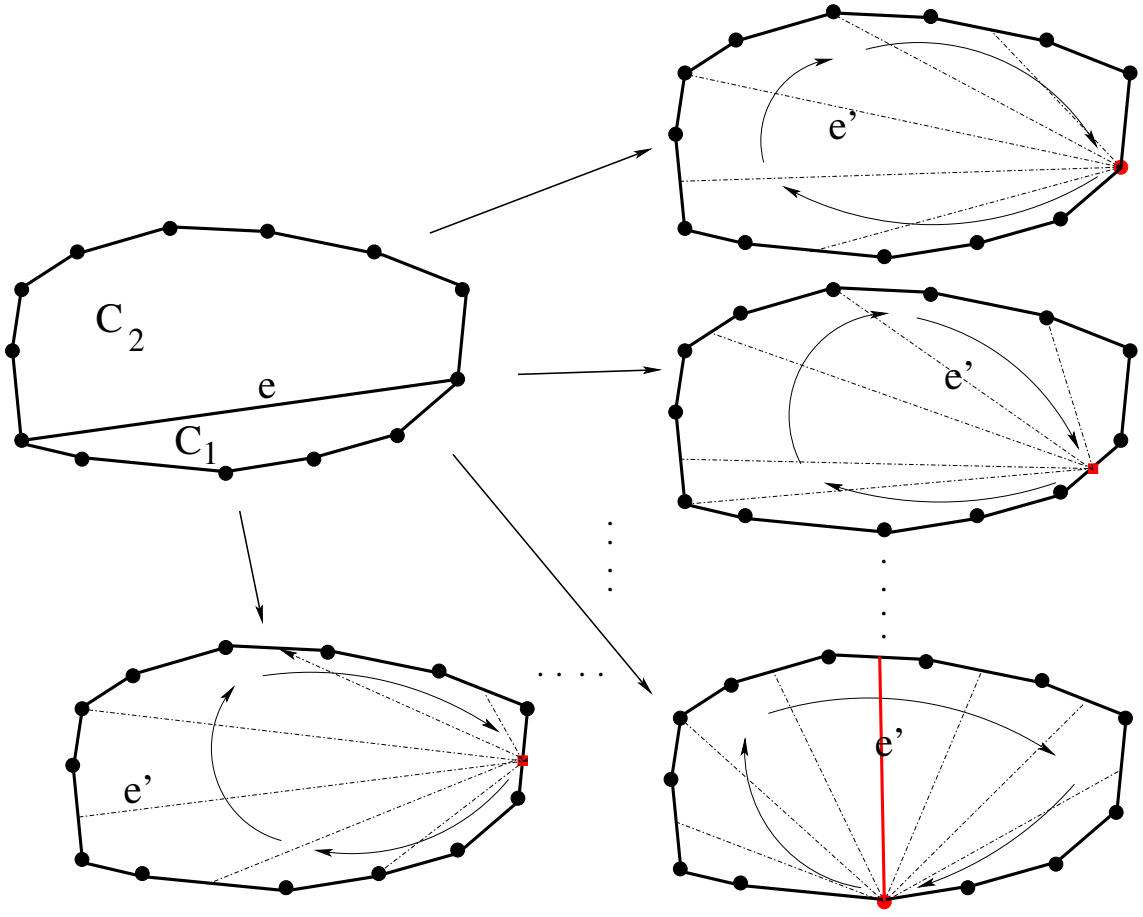

Figure 19: The problem of finding a new swapped edge. Begining with two adjacent cells C_1 and C_2 owning the edge e. Virtual cells C_1', C_2' are created by successively moving each endpoint of virtual edge e' to a node or a mid point edge of $\mathcal{B}(\mathcal{P}^e)$. Initial edge e is (bold black) upside left versus final edge downside right (bold red).

We can distinguish two configurations:

– **Definition 3** *conformal swapping*
If the two new points are existing nodes in (56), we call it ***conformal*** *swap.*

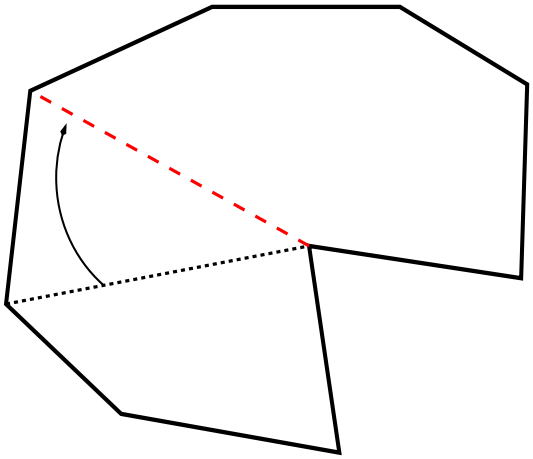

Figure 20: Conformal swap : the new polygons are made up with only **existing** nodes (rotating pair of vertices).

– **Definition 4** *semi-conformal swapping*
If any of the two new points is a mid-edge point, we call it a ***semi-conformal*** *swap.*
we include point on edges (mid-point edge in general)

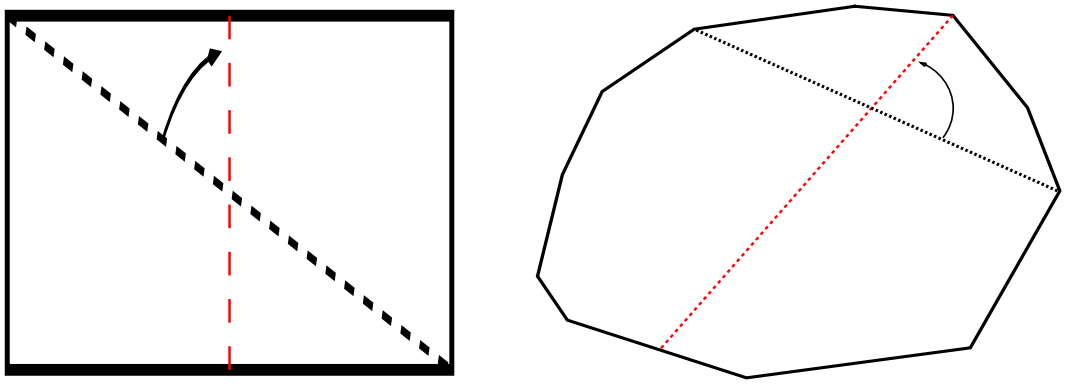

Figure 21: Semi Conformal swap : the new polygons are made up either with existing nodes nor mid-point edge.

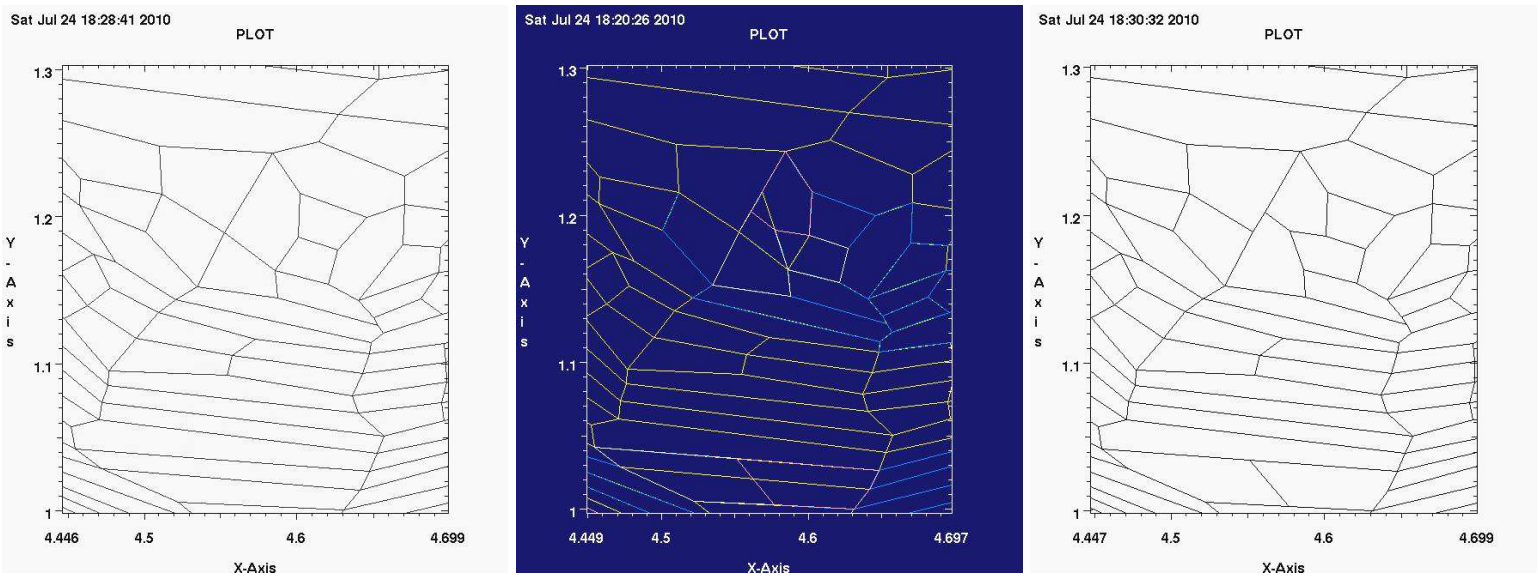

Figure 22: Example of polygonal swapping. Left: Initial mesh, Center: swapped cell and intermediate configuration,, Right: Final mesh

Properties 1 *Properties of extended swapping*
For arbitrary number of extended swapping, the induces mesh modification are that:

- *the cell number is* ***constant****.*
- *the node and edge number* ***may change****.*

Remark 8 *– the underlying mathematical justification is based on* ***tangential discontinuous mesh velocity*** *(on $\mathcal{B}(\mathcal{P}^e)$).*

- *local conservation is easily obtained by a slight extension of self-intersection or basic area swept fluxing algorithm see Figure 23. For first order scheme:*
  - *Standard swept flux scheme [33]:*

$$\begin{aligned} |C^L|^{n+1}Q_L^{n+1} &= |C^L|^nQ_L^n + \delta CQ^*, \\ |C^R|^{n+1}Q_R^{n+1} &= |C^R|^nQ_R^n - \delta CQ^*. \end{aligned} \tag{57}$$

  - *Swept with self intersection flux scheme [25]:*

$$\begin{aligned} |C^L|^{n+1}Q_L^{n+1} &= |C^L|^nQ_L^n + \delta C_1Q^{*,1} + \delta C_2Q^{*,2}, \\ |C^R|^{n+1}Q_R^{n+1} &= |C^R|^nQ_R^n - \delta C_1Q^{*,1} - \delta C_2Q^{*,2}. \end{aligned} \tag{58}$$

In our case, each algebraic area δC in (57) (resp. $\delta C_1, \delta C_2$ in (58)) involve an arbitrary polygonal region that is not necessarily a quadrilater (resp. two simplices). We also recall that $\delta C_1\, \delta C_2 < 0$ and the relationship between (57) and (58) : $\delta C = \delta C_1 + \delta C_2$.

– *In this case, the local patch volume preservation constrain:* $\frac{d}{dt}|\mathcal{P}(\mathrm{e})| = 0$, *(see 53) with* $\mathcal{P}(\mathrm{e}) = C^R \cup C^L$

$$|C^L|^{n+1} + |C^R|^{n+1} = |C^L|^n + |C^R|^n \tag{59}$$

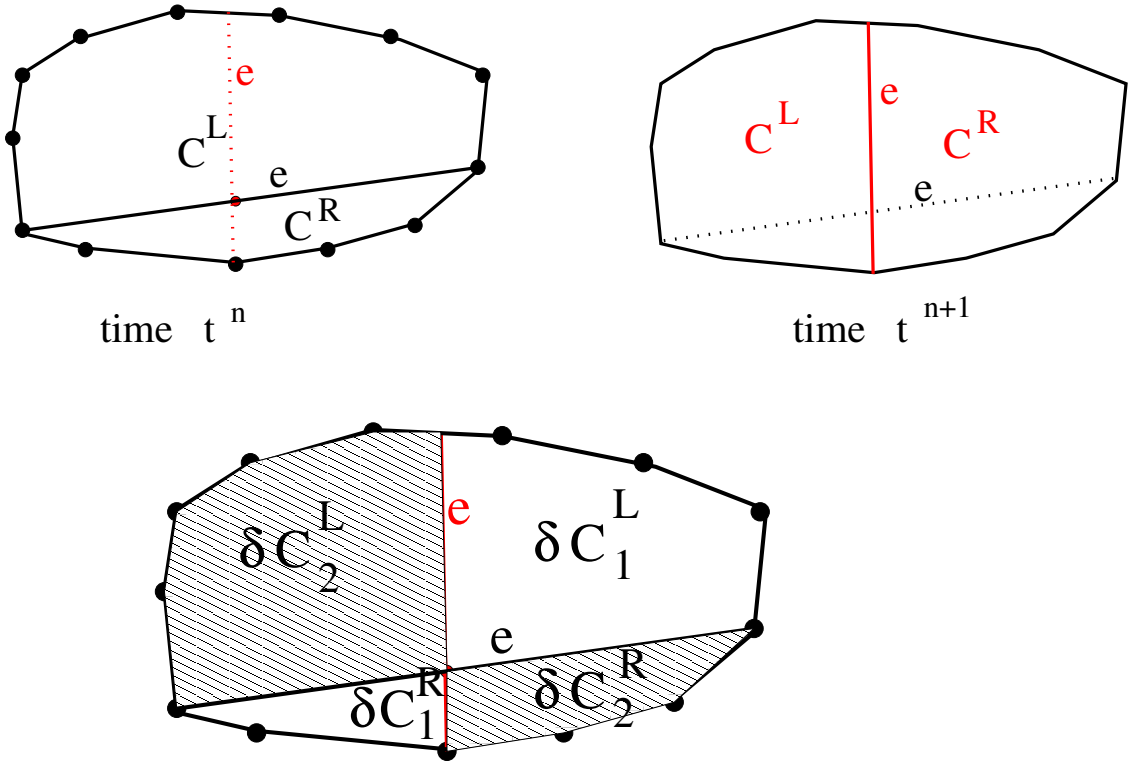

Figure 23: Extended self-intersection (for extended swapping): we use the remap inside the union of two adjacent cells, it is computed by the eventual intersection point appearing during the extended swap see Figure 19, it defines two (and only two) subzonal polygonal regions whose volume can be computed exactly (if we do not consider intersection we recover an extended standard swept flux).

Moreover, for polygons the extended self-intersection is ***exact*** *for the remapping phase if we use the self intersection flux scheme (58).*

– *Sliding mesh edge (see Definition 2) may appear naturally when swapping occured:*

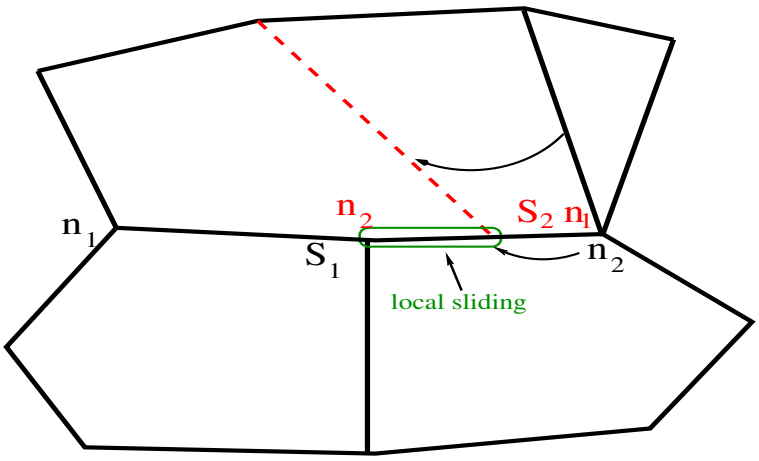

Figure 24: An extended polygonal swapping edge has a sided effect to eventually create a sliding edge.

We summarize some properties of the Discontinuous ALE framework:

Properties 2 *1. $V^{D,Grid}(t,.)$ in $L^\infty(I\!R^d)$ $\Rightarrow$ CFL gives an automatic constraint on remeshing tools (generic local patch of surrounded cells for an edge see Figure 11, 12).*

2. Arbitrary (Convex) polygonal cells.

3. No exact polygon/polygon intersection is needed for remapping.

4. Adding/removing and reconnection of nodes is obtained with a local study.

5. This is a finite volume approach, local conservation is obtained even if discontinuous mesh velocity is involved.

Remark 9 *For h-adaptation, an anisotropic metric based approach [10, 1, 16] can be used. All eligible edge e must verify $|\mathrm{e}|_G \simeq 1$ where $G(\mathbf{x})$ is a strictly positive definite matrix field, let $x_1 = \mathbf{x}(\mathrm{n}_1(\mathrm{e}))$ and $x_2 = \mathbf{x}(\mathrm{n}_2(\mathrm{e}))$:*

$$|\mathrm{e}|_G = \inf_{\gamma(q);\gamma(0)=x_1,\gamma(1)=x_2} \int_0^1 \sqrt{\dot\gamma(q) G(\gamma(q)) \dot\gamma(q)}\ dq. \tag{60}$$

A crude approximation for γ may be $\gamma(q) = \gamma(0) + q(\gamma(1) - \gamma(0))$. We advocate this metric formalism in a future work to control number of cells using edge length.

3.3.4 A Strategy for finite volume Discontinuous ALE

In a practical point of view, the finite volume splitting for discontinuous ALE take the following form:

(A) **Lagrangian** step with a *centered scheme and* all nodes are degree of freedom *and* we do not consider hanging nodes *here, straightening is done if semi-conformity looses geometrical constraint. Approach using special treatment for this exceptional points (see [15]) could also be used.*

(B) **Adaptation** *using refinement/coarsening/extended swapping study (clear and/or add cells) in a semi conformal way. Generalized polygonal edge swapping is performed,* only convexity for new polygonal cells is imposed if needed.

- B_1 refinement and coarse to sub-cell remap (see paragraph 3.3.3 case Refinement).
- B_2 coarsening and remap (see paragraph 3.3.3 case Coarsening).
- B_3 extended swapping and remap by extension of self intersection flux scheme (see paragraph 3.3.3 case Extended swapping).

(C) **Rezoning** (caution when semi-conformity see paragraph 3.3.5 below) and **Remapping** (nothing is changed: polygonal mesh notion with self-intersection flux is used), *no polygon/polygon cell intersection is needed and no dual mesh for momentum remapping is needed.*

(D) Step B_3 is done if rezoning step (C) is not sufficient.

3.3.5 Continuous ALE step with semi conformal cells

(a) **Definition of semi conformal short/medium range** :

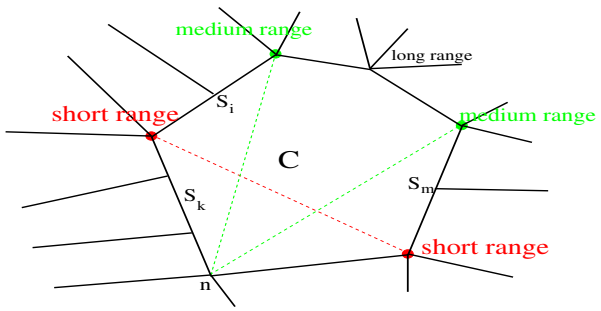

Figure 25: Useful extension of short/medium range [25] for semi-conformal meshes permit to deal with nodal mesh quality control for rezoning.

(b) **Sort the nodes with respect to their level** : (a master node for an edge can be a slave node of another edge).

(c) **Semi-slaves nodes are not taken into account for nodal mesh quality**.

(d) **Welding lines are straighten** when Geometrical constraint is not respected (at each iteration).

We emphasize that the full approach of [25] can be generalized to semi-conformal polygons.

4 Numerical examples

In the following numerical simulation, we perform the computation with the following :

1. Lagrange : if nothing is said, we use the first order version of GLACE [17, 12] or EUCCLHYD [32].
2. ALE : Rezoning applied with barycentric smoother (eventually with anisotropic weights) coupled with Escobar and al [20] with the approach of [25]. The remapping step is done with self intersection flux.

4.1 Sod shock tube

We consider the classical Sod shock tube problem on a cartesian $50\times$ 50 initial cartesian mesh.

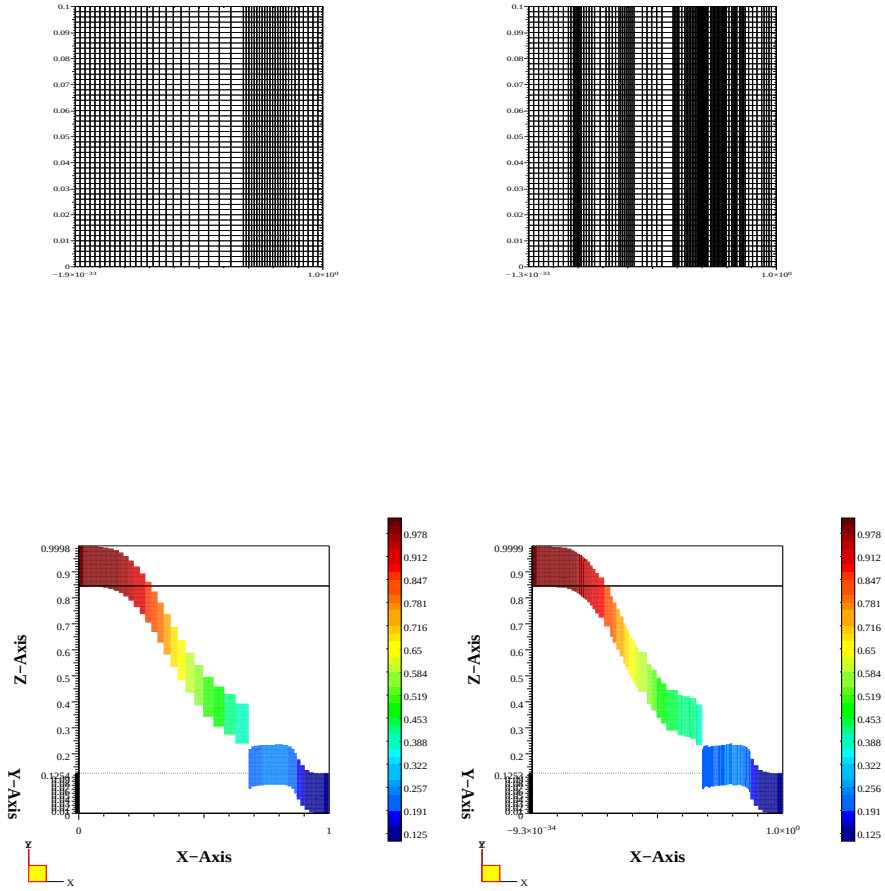

Figure 26: Sod shock tube problem, (above) mesh and (below) density at final time. Left: Pure Lagrangian (mesh and density), Right: Lagrangian with h-adaptation (layer by layer)

4.2 Sedov

In this case, we solve the Sedov problem. The initial condition is given by $(\rho^0, P^0, \mathbf{U^0}) = (1, 10^{-6}, \mathbf{0})$ and $\gamma = 1.4$. The pressure in cell C containing the origin is such that, see [31],

$$P_c = (\gamma - 1)\rho_C \frac{\varepsilon^0}{|C|} \tag{61}$$

where $\varepsilon^0 = 0.244816$ so that the solution consists of a diverging shock whose front is located at radius R=1 at time t=1. We consider Lagrange with ALE barycentric smoothing on 51×51 initial cartesian mesh. At some times we begin our DiscALE adaptation (without swapping) see Figure 27.

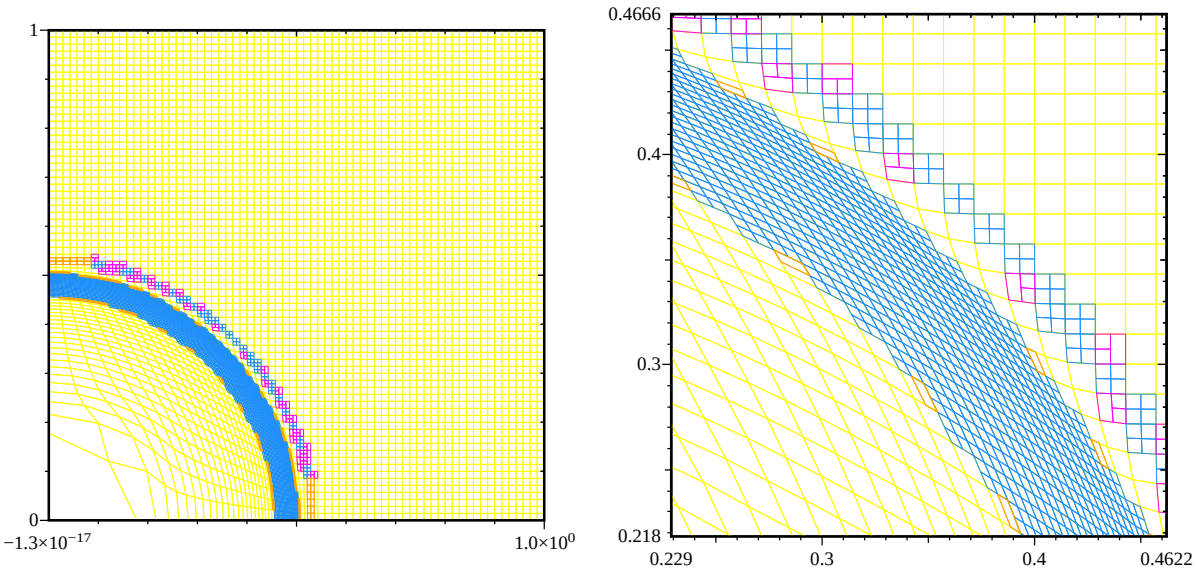

Figure 27: Sedov Test Case. Left standard ALE enhanced with DiscALE, Right Zoom on different type of adapted cells : isotropic (blue), quasi-anisotropic (magenta), anisotropic (orange).

Tri-materials Lag+Adaptation+ALE. Let an initial regular cartesian grid, with three perfect gases (with different γ) at rest in three different zones see Figure below:

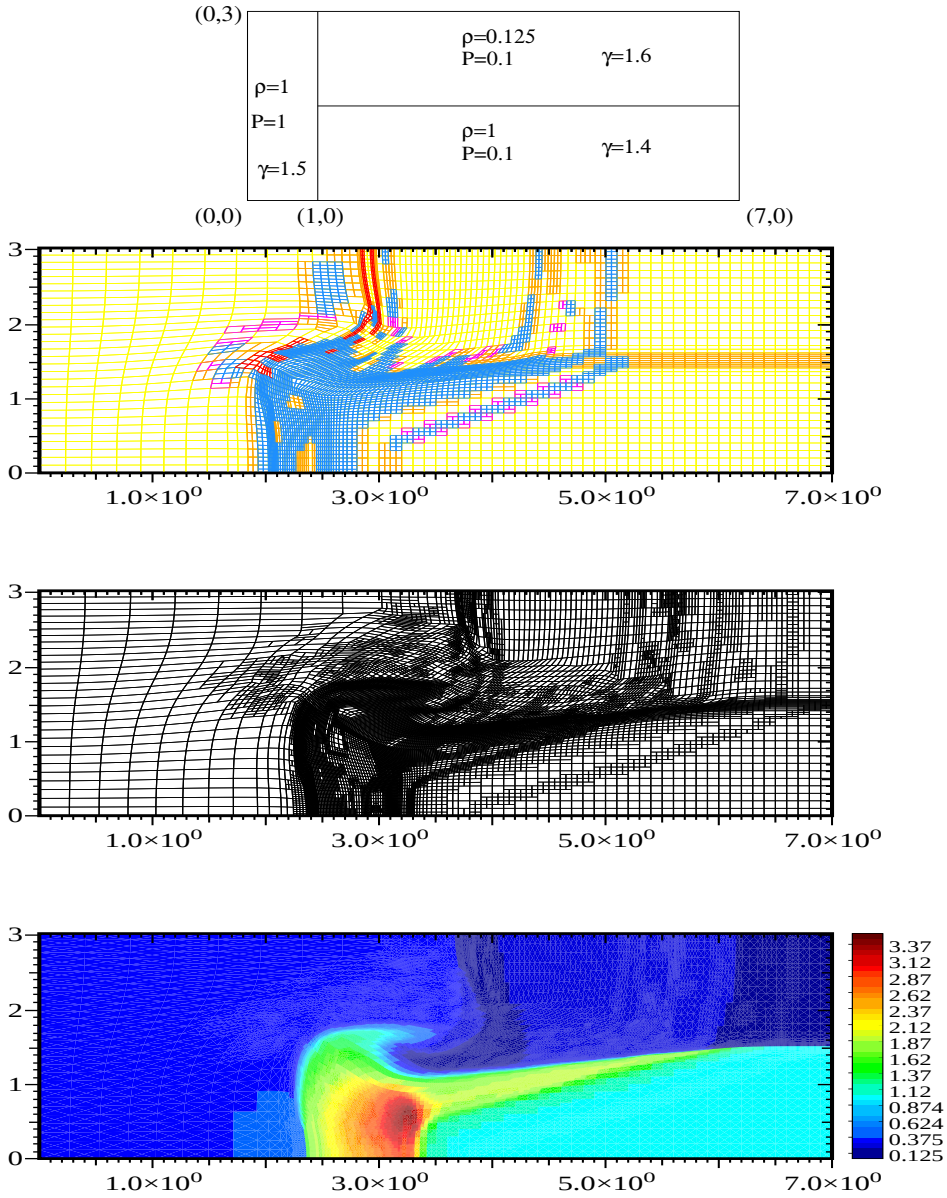

Figure 28: Tri-Materials test case. Up: different type of local cell by cell refinement (yellow mesh is the one before refinement) at time t=2.5, middle: the computational adapted mesh at time t=3, and down : density at time t=3.

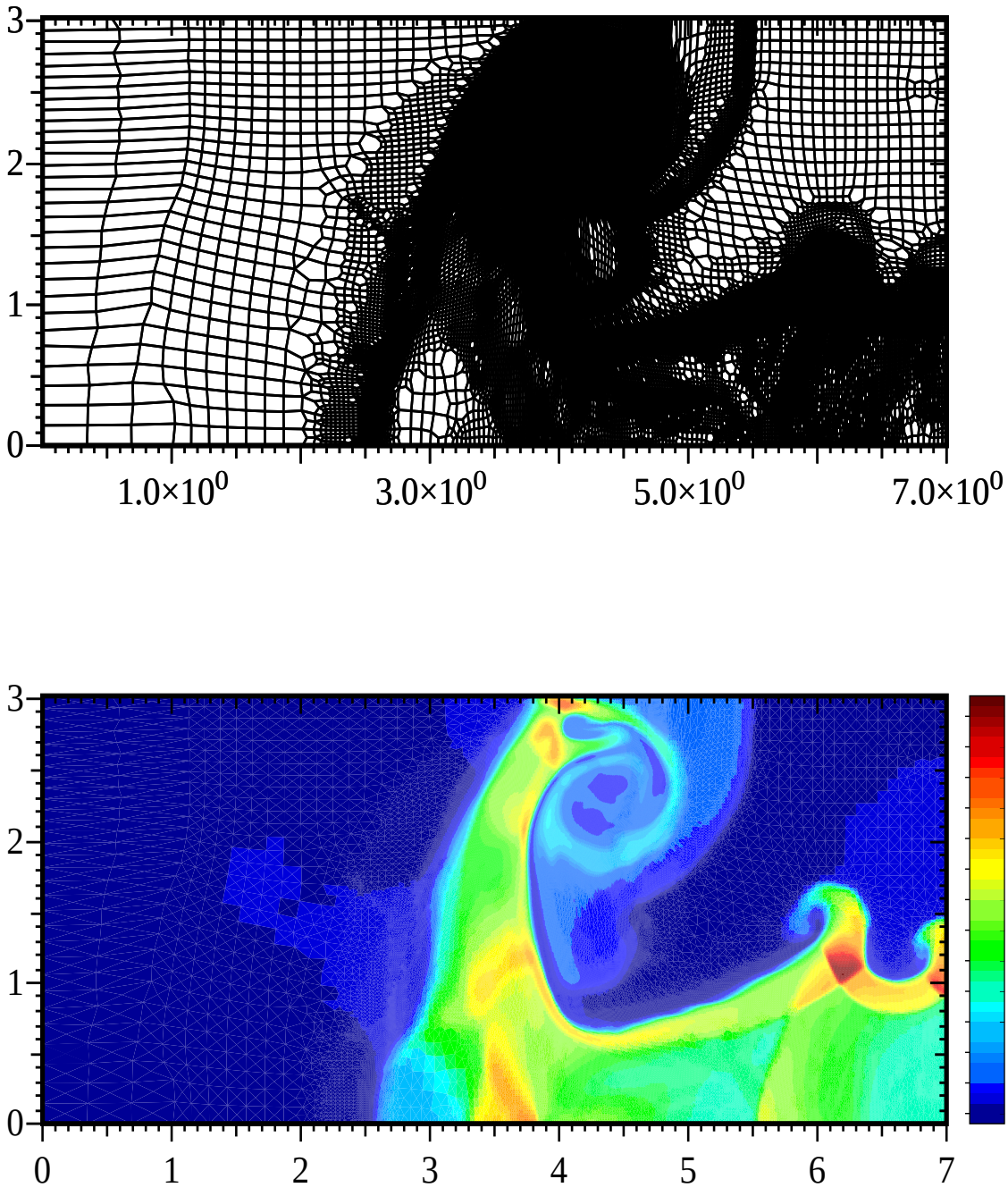

Figure 29: Density and mesh at time t=10. Extended swapping on polygons (see (56) in Figure 19) has been enabled. Note that the initial cartesian mesh possess polygons with more than four nodes. Connectivity is truly arbitrary throughout the calculation and is not known in advance.

5 Conclusion and prospects

We have presented a formulation that encompass existing ALE framework (Lagrange, rezoning and remap) on arbitrary conformal or semi conformal polygonal cells. A discontinuous mesh velocity is introduced to take into account mesh refinement, coarsening or extended swapping, a consequence is the modeling of h-adaptation in numerical simulations. The discontinuous frame permits to deal with node duplication or collapsing. For a computational point of view, we resume properties of our approach:

(1) Centered finite volume Lagrangian hydrodynamics schemes (GLACE, EUCCLHYD, etc), arbitrary polygonal cells can be handled, second order space/time scheme (with double limiter on specific variable).

(2) For refinement, the local AMR-ALE is recover as a *special case (Discontinuous ALE with short range).*

(3) Coarsening by cleaning edges is generic, edge to node transformation is permitted.

(4) Edge swapping has been extended to polygonal/non conformal cells (sliding edge may appear).

(5) Layer refinement and coarsening are just a consequence of the symmetry of the flow.

(6) No exact mesh intersection is needed, only local remapper (swept area or self intersection at most) is used (at least in case of single material).

It appears that h-adaptation with reconnection can be seen as a discretization of (splitted) ALE version with discontinuous kinematic field (see previous preliminary works [26, 27]). Future works will include sharper coupling with existing approach (control of edge length with a prescribed metric, nodal mesh quality with physical weights). Extension to conical meshes is theoretically possible as well as multi-materials ALE.

The author is grateful to J.F. Babadjan, V. Millot, F. James for fruitful discussions on the discontinuous mathematical framework.

References

[1] F. Alauzet and P.-J. Frey. Anisotropic mesh adaptation for cfd computations. *Comput. Meth. Appl. Mech. Eng.*, 194:5068–5082, 2005.

[2] L. Ambrosio. Transport equation and cauchy problem for bv vector fields. *Inventiones Math.*, 158:227–260, 2004.

[3] L. Ambrosio, N. Fusco, and D. Pallara. *Functions of bounded variation and free discontinuity problems*. The Clarendon Press, Oxford University Press, New York, 2000.

[4] R.W. Anderson, N.S. Elliott, and R.B. Pember. An arbitrary lagrangian-eulerian method with adaptive mesh refinement for the solution of the euler equations. *Journal of Computational Physics*, 199(2):598–617, 2004.

[5] H. Askes, E. Kuhl, and P. Steinmann. An ale formulation based on spatial and material settings of continuum mechanics. part 2: Classification and applications. *Comput. Methods Appl. Mech. Engrg.*, 193:4223–4245, 2004.

[6] F.P.T Baaijems. An u-ale formulation of 3-d unsteady viscoelastic flow. *Inter. Jour. Num. Methods Engrg.*, 36:1115–1143, 1993.

[7] E. Bernard, S. Del Pino, E. Deriaz, B. Després, K. Jurkova, and F Lagoutière. Lagrangian method enhanced with edge swapping for the free fall and contact problem. In *ESAIM: Proc.*, volume 24, pages 46–59, 2008.

[8] F. Bouchut and F. James. One-dimensional transport equations with discontinuous coefficients. *Nonlinear Analysis, TMA*, 32(7):891–933, 1998.

[9] F. Bouchut, F. James, and S. Mancini. Uniqueness and weak stability for multidimensional transport equations with one-sided lipschitz coefficients. *Ann. Scuola Norm. Sup. Pisa Cl. Sci.*, 5(4):1–25, 2005.

[10] H. Bourouchaki, P.-L. George, F. Hecht, P. Laug, and E. Saltel. Delaunay mesh generation governed by metric specifications. *Finite Elem. Anal. Design*, 25:61–83, 1997.

[11] H. Brezis. *Analyse Fonctionnelle*. Masson, 1983.

[12] G. Carre, S. Del Pino, B. Despres, and E. Labourasse. A cell-centered lagrangian hydrodynamics scheme on general unstructured meshes in arbitrary dimension. *Jour. of Comp. Physic.*, 228:5160–5183, 2009.

[13] J. Cheng and C.W. Shu. A third order conservative lagrangian type scheme on curvilinear meshes for the compressible euler equations. *Comm. on comput. phys*, 4(5):1008–1024, 2008.

[14] A. Chorin and J. Marsden. *A Mathematical Introduction to Fluid Mechanics*. Springer Verlag, 1992.

[15] A. Claisse, B. Després, E. Labourasse, and F. Ledoux. A new exceptional points method with application to cell-centered lagrangian schemes and curved meshes. *J. Comput. Phys.*, 231:4324–4354, 2012.

[16] S. Del Pino. Metric-based mesh adaptation for 2d lagrangian compressible flows. *Comput. Meth. Appl. Mech. Eng.*, 230(5):1793–1821, 2011.

[17] B. Després and C. Mazeran. Lagrangian gas dynamics in two dimensions and lagrangian systems. *Arch. Rational Mech. Anal.*, 178:327–372, 2005.

[18] J. Donea, A. Huerta, J.Ph. Ponthot, and A. Rodríguez-Ferran. *Arbitrary Lagrangian-Eulerian Methods*, volume 1, chapter 14. in Encyclopedia of Computational Mechanics, John Wiley & Sons, 2004.

[19] G. Duvaut. *Mécanique des milieux continus*. Coll. Math. appl. pour la maîtrise, MASSON, 1990.

[20] J.M. Escobar, E. Rodriguez, R. Montenegro, G. Montero, and J.M. Gonzalez-Yuste. Simultaneous untangling and smoothing of tetrahedral meshes. *Comp. Meth. in Applied Mechanics and Engineering*, 192(25):2775–2787, 2003.

[21] O. Faugeras and J. Gomes. Representing and evolving smooth manifolds of arbitrary dimension embedded in rn as the intersection of n hypersurfaces : The vector distance functions. *HAL 2000*, pages 1–13, 2000.

[22] O. Faugeras and J. Gomes. Using the vector distance functions to evolve manifolds of arbitrary codimension. *Proceedings of the Third International Conference on Scale-Space and Morphology in Computer Vision*, pages 1–13, 2001.

[23] P.J. Frey and P.L. George. *Mesh generation. Application to finite elements. Hermes Science Publ., Paris*. Oxford, 2000.

[24] C. W. Hirt, A. A. Amsden, and J. L. Cook. An arbitrary lagrangian-eulerian computing method for all flow speeds. *J. Comput. Phys.*, 135:203–216, 1997.

[25] P. Hoch. An arbitrary lagrangian-eulerian strategy to solve compressible fluid flows. HAL 2009, http://hal.archives-ouvertes.fr/hal-00366858/PDF/ale2d.pdf, March 2009.

[26] P. Hoch. Semi-conformal polygonal mesh adaptation seen as discontinuous grid velocity formulation for ale simulations. Conference on Numerical methods for multi-material fluid flows MULTIMAT'09 Pavia, www.math.univ-toulouse.fr/HYDRO, 2009.

[27] P. Hoch. A two-dimensional discontinuous ale(discale) finite volume framework on arbitrary unstructured conical meshes. Conference on Numerical methods for multi-material fluid flows MULTIMAT'11 Arcachon, http://multimat2011.celia.u-bordeaux1.fr/Multimat2011/Tuesday_AM/Hoch.pdf, 2011.

[28] P. Hoch, S. Marchal, Y. Vasilenko, and A. A. Feiz. Non conformal adaptation and mesh smoothing for compressible lagrangian fluid dynamics. In *ESAIM Proc*, volume 24, pages 111–129, 2008.

[29] P.L. Lions and R.J. Di Perna. Ordinary differential equations, transport theory and sobolev spaces. *Invent. math*, 98:511–547, 1989.

[30] R. Loubère, P.H. Maire, M. Shashkov, J. Breil, and S. Galera. Reale: A reconnection-based arbitrary-lagrangian-eulerian method. *Journal of Computational Physics*, 229(12):4724–4761, 2010.

[31] P.-H. Maire. *Contribution à la modélisation numérique de la Fusion par Confinement Inertiel*. Hdr, Université Bordeaux I, February 2011.

[32] P.H. Maire, R. Abgrall, J. Breil, and J. Ovadia. A cell-centered lagrangian scheme for two-dimensional compressible flow problems. *SIAM J.Sci.Comput.*, 29:1781–1824, 2007.

[33] L.G. Margolin and M. Shashkov. Second order sign preserving remapping on general grids. *J.Comp.Phys*, 184:266–298, 2003.

[34] J.M. Morrell, P.K. Sweby, and A. Barlow. A cell by cell anisotropic adaptive mesh ALE scheme for the numerical solution of the Euler equations. *Journal of Computational Physics*, 226:1152–1180, 2007.

[35] J.M. Morrell, P.K. Sweby, and A. Barlow. A cell by cell anisotropic adaptive mesh ale method. *Int. J. Num. Meth. in Fluids*, 56:1441–1447, 2008.

[36] M. Rascle and F. Poupaud. Measure solutions to the linear multidimensional transport equation with non smooth coefficients. *Comm. Part. Diff. Eq.*, 22:337–358, 1997.